



HAL
open science

Structure of Strontium Aluminosilicate Glasses from Molecular Dynamics Simulations, Neutron Diffraction and Nuclear Magnetic Resonance Studies

Thibault Charpentier, Kirill Okhotnikov, Alexey Novikov, Louis Hennet,
Henry Fischer, Daniel Neuville, Pierre Florian

► **To cite this version:**

Thibault Charpentier, Kirill Okhotnikov, Alexey Novikov, Louis Hennet, Henry Fischer, et al.. Structure of Strontium Aluminosilicate Glasses from Molecular Dynamics Simulations, Neutron Diffraction and Nuclear Magnetic Resonance Studies. *Journal of Physical Chemistry B*, 2018, 122, pp.9567-9583. 10.1021/acs.jpcc.8b05721 . cea-01878549

HAL Id: cea-01878549

<https://cea.hal.science/cea-01878549>

Submitted on 21 Sep 2018

HAL is a multi-disciplinary open access archive for the deposit and dissemination of scientific research documents, whether they are published or not. The documents may come from teaching and research institutions in France or abroad, or from public or private research centers.

L'archive ouverte pluridisciplinaire **HAL**, est destinée au dépôt et à la diffusion de documents scientifiques de niveau recherche, publiés ou non, émanant des établissements d'enseignement et de recherche français ou étrangers, des laboratoires publics ou privés.

Structure of Strontium Aluminosilicate Glasses from Molecular Dynamics Simulations, Neutron Diffraction and Nuclear Magnetic Resonance Studies

Thibault Charpentier^{1*}, Kirill Okhotnikov¹, Alexey N. Novikov², Louis Hennet², Henry E. Fischer³, Daniel R. Neuville⁴, Pierre Florian²

1. NIMBE, CEA, CNRS, Université Paris-Saclay, CEA Saclay, 91191 Gif-sur-Yvette cedex, France.
2. CEMHTI UPR3079 CNRS, Univ. Orléans, F-45071 Orléans, France
3. Institut Laue-Langevin, 38042 Grenoble Cedex 9, France
4. IPGP UMR7154 CNRS, Géomatériaux, Paris Sorbonne Cité, 75005 Paris, France

* thibault.charpentier@cea.fr

Abstract

The structure of strontium glasses with composition $(\text{SiO}_2)_{1-2x}(\text{Al}_2\text{O}_3)_x(\text{SrO})_x$ ($R=[\text{SrO}]/[\text{Al}_2\text{O}_3]=1$) and $(\text{SiO}_2)_{1-4x}(\text{Al}_2\text{O}_3)_x(\text{SrO})_{3x}$ ($R=3$) have been explored experimentally over both short and intermediate length scales using neutron diffraction, ^{27}Al and ^{29}Si nuclear magnetic resonance and classical molecular dynamics simulations in model systems containing around 10000 atoms. We aim at understanding the structural role of aluminum and strontium as a function of the chemical composition of these glasses. Short- and medium-range structure such as aluminum coordination, bond angle distribution, $Q^{(n)}$ distribution and oxygen speciation have been systematically studied. Two potential forms of the repulsive short-range interactions have been investigated, namely the Buckingham and Morse forms. The comparison allows us to derive general trends independent of the particular choice of the potential form. In both cases, it is found that aluminum ions are mainly four-fold coordinated and mix with the silicon network favoring Al/Si mixing in terms of Al-O-Si linkages. For the $R = 1$ glass series, despite the full charge compensation ($[\text{SrO}]=[\text{Al}_2\text{O}_3]$), a small fraction of five-fold aluminum is observed both experimentally and in MD simulations, while the concentration of six-fold aluminum is negligible. MD shows that

five-fold aluminum units AlO_5 preferentially adopt small rings configuration and link to tricoordinated oxygen atoms which population increases with the aluminum content and are mainly found in OAl_3 and OAl_2Si configurations. The modeled Sr speciation mainly involves SrO_7 and SrO_8 polyhedra, giving a range of average Sr^{2+} coordination numbers between 7 and 8 slightly dependent on the short-range repulsive potential form. A detailed statistical analysis of the T-O-T' (T,T'=Al,Si), accounting for the population of the various oxygen speciation, reveals that both potentials predicts a nearly identical Al/Si mixing.

1. Introduction

Thanks to their good mechanical and high chemical durability, aluminosilicate glasses have found wide industrial and technological applications. In these respects and also because of their importance in geoscience due to their presence in the Earth's magma, alkali-earth aluminosilicate have been experimentally and computationally thoroughly investigated, but almost exclusively with Ca^{++} cations (CAS system), see for example Refs. ¹⁻¹⁰ where the fully charge balanced tectosilicate join has been the most studied. Despite the full charge compensation, intrinsic defects such as non-bridging oxygens^{1,11-14} or higher coordinated states of aluminium ($\text{AlO}_{5,6}$)^{10,12,15} that can be directly observed and easily quantified from ²⁷Al NMR, are observed. In order to explain compensation of the excess of charge, tricoordinated oxygens (also referred to as tricluster oxygens or triply-bonded oxygens) have also been invoked^{8,16,17} but their existence is still mainly supported by MD simulations^{4,8,18-20} only. Indeed quantum chemical studies have shown that such species could not be resolved by ¹⁷O NMR spectroscopy.²¹⁻²³

Conversely to CAS, the structure of strontium aluminosilicate glasses (SAS) have been only scarcely studied, despite their high potential for developing new materials, such a

transparent ceramics,^{24,25} high temperature sealants²⁶ and refractory materials.^{27,28} RMC studies of the glass SrO-Al₂O₃-4SiO₂²⁹ suggested a non-homogenous spatial distribution of Sr atoms with a Sr-O distance which is longer in aluminosilicate (2.7 Å) than in binary silicate (2.55 Å) glasses, in agreement with analogous crystal structures SrAl₂Si₂O₈ and SrSiO₃. This pointed out the dominant role of Sr as charge compensator in SAS on the [Al₂O₃=SrO] join (R = 1). X-ray analysis in borosilicate glasses showed an average Sr-O distance of 2.53 Å with coordination number ranging from 4 to 6.³⁰ More recently,³¹ a systematic study of the R=1 glass compositions showed that Al is predominantly in tetrahedral form, with a maximum of 5% in fivefold coordinated units. Strontium coordination number was found to be around 9 (from Sr K-edge XAS).

Thus, including strontium in a more systematic way is of interest to complete the aluminosilicate glass structure frame. This will also complete a recent attempt to rationalize the effect of the cation field strength on the appearance of high coordination AlO_{5,6} sites,³² even at exact charge balance condition. Generally, it was observed that the tendency of the modifier cations to charge balance AlO₄ units has decreasing probability with increasing ionic field strength as higher field strength often promotes the appearance of negative charge such as non-bridging oxygens or highly-charged Al-O-Al groups.³³ The exact role of high coordination states of aluminum to the global charge balance, often accompanied by the appearance of tricoordinated oxygens (denoted O^[3]) and/or non-bridging oxygens (denoted O^[1]), still need to be clarified. This highlights the three mechanisms that have been proposed for local charge compensations in aluminosilicate glasses. The first one is the formation of highly coordinated aluminums such as AlO₅ and AlO₆. The second mechanism postulates the idea of tricoordinated oxygens (also referred to as triclusters or triply bonded oxygens), involving the sharing of oxygen among three network forming units (SiO₄, AlO₄ but also

AlO₅), as corroborated directly by many MD studies and indirectly by NMR studies. The third one relies on the formation of (non-stoichiometric) non-bridging oxygens which have been observed in potassium, calcium and barium aluminosilicates but in amounts decoupled from the concentration of AlO₅ species.³⁴ In addition, it has been shown recently experimentally that the speculated Al-O^[1] bonds also form in rare-earth aluminosilicate glasses.^{35,36}

In this work, two strontium aluminosilicate glass series are examined: the first is on the exact charge compensation line ([SrO]/[Al₂O₃]=1) with compositions (SiO₂)_{1-2x}(Al₂O₃)_x(SrO)_x ; in the second, strontium oxide is in excess ([SrO]/[Al₂O₃]=3) with compositions (SiO₂)_{1-4x}(Al₂O₃)_x(SrO)_{3x}. These glasses are investigated theoretically by means of molecular dynamics simulations using two forms of potential models made by two-body interactions. Although these potential sets predict reasonable glass structures with respect to the neutron diffraction and nuclear magnetic resonance data, both featuring an increasing concentration of both high coordination aluminum units AlO_{5,6}, tricoordinated and non-bridging oxygen atoms with the aluminum content, they are found to differ mainly in the relative populations of the various oxygen species O^[n] (n=1-3) whereas Sr coordination numbers and Al/Si mixing are similar. This first allows us to draw some general conclusions about the role of the interaction potential sets. Secondly, we determine the intimate relationships that exists between the two main charge compensation mechanisms: high coordinated aluminum units and O^{[1],[3]} oxygens.

2. Materials and Methods

2.1 Starting Materials. Strontium aluminosilicate samples were made by a traditional melt-quenching procedure and characterized (composition, homogeneity, density) as described in ref³¹ for the R = 1 glass series. For glass samples that could not be obtained using this

procedure (SA50.25 and SA75.12), small glass spheres were prepared employing an aerodynamics levitation device coupled to two CO₂ lasers.³⁷ Glasses are named SAxx.yy where xx and yy are the SiO₂ and Al₂O₃ content in mol%, respectively.

2.2 Nuclear Magnetic Resonance. ²⁷Al MAS NMR spectra have been collected on a Avance III Bruker 850 MHz (20.0T) spectrometer operating at a Larmor frequency of 195.5 MHz and using a 2.5 mm Bruker CPMAS probe at a spinning frequency of 30 kHz. A short single pulse excitation of 0.4 us, i.e. less than $\pi/18$, was used to ensure quantitiveness (i.e., in order to avoid non-homogeneous excitation of the line because of dependence of the excitation efficiency upon quadrupolar interaction for long pulse length) for with a recycle delay of 0.15 s. Triple Quantum MQMAS spectra were acquired using a shifted Echo pulse sequence.³⁸ Chemical shifts are referenced to a 1M aqueous Al(NO₃)₃ solution.

²⁹Si MAS NMR spectra have been collected on a Avance I Bruker 300 MHz (7.05T) spectrometer operating at a Larmor frequency of 59.5 MHz and using a 4mm Bruker CPMAS at a spinning frequency of 10 kHz. Data were acquired a CPMG pulse sequence³⁹⁻⁴¹ with a recycle delay of 200s and typically 256 scans. 16 echoes with an echo delay of 6 ms between consecutive 180° pulses were accumulated. They were then summed up and Fourier transformed to obtain the spectra. The spectra are referenced to an external tetrakis(trimethylsilyl)silane (TKS) sample, for which the highest intensity peak was positioned at -9.9 ppm from that of TMS.

All data were processed and fitted using an in-house written software (T. Charpentier), including shortest-path analysis for the search of primary rings.

2.3 Neutron diffraction. The neutron diffraction measurements were carried out on the D4C diffractometer⁴² at the Institute Laue Langevin (ILL) in Grenoble (France). A neutron

wavelength (λ) of 0.4985 Å was selected for the measurements. Glass samples (3 to 4mm in diameter) were placed into a vacuum chamber that was pumped down to a pressure of 10^{-4} mbar. The total duration of each run was about 3 hours, including the displacement of the detector.

The procedure for the data treatment is described in details in ref.⁴³ The structure factors were obtained using the program CORRECT⁴⁴ which corrects the data for attenuation, background, multiple scattering and inelasticity (Placzek) effects. Finally, the total pair distribution functions were then calculated from the structure factors by the Fourier transform:

$$G(r) - 1 = \frac{1}{2\pi^2 r \rho_0} \int_0^\infty [S(Q) - 1] Q \sin(Qr) dQ \quad (1)$$

where ρ_0 denotes the atomic number density. The later is calculated using densities measured with the Archimedean method applying toluene as immersion liquid.

2.4 Molecular Dynamics Simulations. A single model for each composition was generated as described in **Table 1**. MD simulations were performed with the DL_POLY program.^{45,46} Two pairwise potential models were compared; both includes the long range Coulombic contributions with partial-charge rigid-ion model. In the first set, short range interactions were chosen in the Buckingham form:

$$V(r) = A_{ij} \exp(-r/\rho_{ij}) - C_{ij}/r^6 \quad (2)$$

In the second set, a Morse function was chosen including a repulsion term C/r^{12} as:

$$V(r) = D_{ij} \left[\{1 - e^{-a_{ij}(r-r_0)}\}^2 - 1 \right] - C_{ij}/r^{12} \quad (3)$$

Parameters A_{ij} , ρ_{ij} , C_{ij} , D_{ij} , a_{ij} and r_0 are given in **Table 2** and **Table 3**. Morse parameters were developed by Pedone et al.⁴⁷ and Buckingham ones are from previous studies,⁴⁸⁻⁵⁰

except for Sr-O interaction for which new parameters were derived as described by fitting DFT calculations⁵¹ as described in the Supporting Information. Buckingham potential sets were corrected at very short range as described in Ref.⁵¹

Coulombic interactions were calculated using the Ewald Sum summation method with a precision of 10^{-6} , a real-space cutoff of 9 Å to evaluate repulsive forces with periodic boundary conditions and 12 Å for the Coulombic interactions. A time step of 0.5 fs was used. The Melt and Quench method was employed to generate the glass structures. Starting from random initial structures (generated with shortest bond length constraints between atom pairs), they were melted during 100 ps at 3500 K to remove memory effects and then cooled subsequently to 300 K in steps of 100 K. At each temperature, a 50 ps relaxation was allowed in the NVT ensemble (using a Berendsen thermostat with a 1 ps relaxation time constant) followed by 50ps in the NVE ensemble. This annealing protocol leads to a nominal quenching rate of 1 K/ps.

Data collection was performed every 20 steps during the last 50000 steps of an extended 200 ps MD run in the NVE ensemble at 300 K. Data were processed and analyzed with an in-house written code (T. Charpentier). Coordination numbers were calculated using cutoff radius values of 2.2 Å for Si-O and Al-O, and 3.5 Å for Sr-O, as determined from the minimum after the first peak maximum of the partial radial distribution function.

Table 1. Compositions, Densities and Simulation Cell Information of the Simulated Glasses

Glass	Number of atoms				Density (g/cm ³)	Edge length (Å)
	Al	O	Si	Sr		
R=1						
SA26.37	2160	5856	768	1080	3.298	51.3024
SA33.33	1968	5904	984	984	3.211	51.3232
SA42.29	1800	6200	1300	900	3.132	51.8642
SA50.25	1600	6400	1600	800	3.021	52.3286
SA57.21	1400	6500	1850	700	2.928	52.4819

SA63.18	1200	6500	2050	600	2.837	52.4319
SA75.12	800	6575	2475	425	2.636	52.7898
R=3						
SA33.17	1200	5925	1175	1175	3.628	52.4750
SA42.14	1008	6120	1512	1584	3.482	52.6690
SA50.12	850	6175	1775	1350	3.349	52.3816
SA60.10	728	6552	2184	1092	3.139	52.9982

Table 2. Parameters of the Buckingham Potentials

Pair	A (eV)	ρ (Å)	C (eV.Å ⁶)	Ref
Al ^{+1.8} -O ^{-1.2}	12201.417	0.195628	31.997	(Du, 2009)
O ^{-1.2} -O ^{-1.2}	1844.7458	0.343645	192.58	
Si ^{+2.4} -O ^{-1.2}	13702.905	0.193817	54.681	
Sr ^{+1.2} -O ^{-1.2}	4314.907	0.312116	377.478	This work

Table 3. Parameters of the Morse Potentials from ref 47

Pair	D (eV)	a (Å)	r_0 (Å ²)	C (eV. Å ¹²)
Al ^{+1.8} -O ^{-1.2}	0.361581	1.900442	2.164818	0.9
O ^{-1.2} -O ^{-1.2}	0.042395	1.379316	3.618701	22.0
Si ^{+2.4} -O ^{-1.2}	0.340554	2.0067	2.1	1.0
Sr ^{+1.2} -O ^{-1.2}	0.019623	1.886	3.32833	3.0

3. Results and Discussion

3.1 Nuclear Magnetic Resonance Spectroscopy. ²⁷Al MAS NMR spectra of the R=1 glass series have been recently reported³¹ but for the sake of completeness they will be shown here as well, along with the R=3 glass series spectra; MQMAS spectra for both glass series detailed are given in the Supporting Information. Moreover although previous³¹ and present studies use the same model to simulate the same one-dimensional data set, the simulation procedure used here is slightly different as it relies on the MQMAS experiments as well and gives therefore an evaluation of the uncertainties in determining the NMR parameters.

In Figure 1 are shown the ²⁷Al MAS NMR spectra, the variations of the mean isotropic chemical shift δ_{iso} and mean quadrupolar coupling constant C_Q against the glass composition. The mean values of the NMR parameters were calculated from the NMR parameters distribution extracted from the MAS using constraints from the MQMAS spectra,

as detailed in the Supporting Information. Note that for the SA63.18 glass, a small impurity is seen at about 10 ppm (α -Al₂O₃).

If for both glass series, R = 1 and R = 3, a dominant AlO₄ speciation is clearly observed, a small amount of AlO₅, ranging from 1 to 6% (Figure 2) is clearly revealed by MQMAS spectroscopy (see spectra in Supporting Information). This is quite surprising for the R = 3 series as it could have been anticipated that the higher SrO concentration would have facilitated a full charge compensation of AlO₄ units.

Concerning the dominant AlO₄ units, both glass series exhibit a clear decrease of the isotropic chemical shift δ_{iso} against the ratio $r=Si/Al$ with similar averaged slopes (see dashed line in Figure 1, right panel) of about -4.8 ppm/Si and -4.9 ppm/Si for R=1 and R=3, respectively. This variation can be safely ascribed to Al/Si mixing: larger (resp. smaller) δ_{iso} corresponds to higher connectivity with aluminum (resp. silicon), as already observed and quantified in gehlenite.⁵² Such values of the slope are in good agreement with previously predicted values between -3 to -5 ppm in aluminosilicate glasses⁶ and experimentally observed value of -3 ppm in gehlenite.⁵² The ²⁷Al quadrupolar coupling constant C_Q values vary in two steps: values first decrease for low silica content (<40%) to reach in a second step a plateau for silica-rich compositions. For low silica content, higher Al-O-Al connectivity requires a larger amount of charge compensators in the surrounding of Al atoms which results in a larger local electric field gradient (EFG), thus larger C_Q . The origin of the overall reduction of C_Q values from the R=1 to R=3 glass compositions is less clear. The presence of a higher amount of non-bridging oxygen atoms could help aluminum atoms in the system to adopt less distorted environments because of diminished constraints arising from reduced bonding with neighboring units (more depolymerized network). Further discussion regarding

these aspects will be presented in a forthcoming paper combining present MD simulations with DFT-NMR calculations, using the methodology presented in Ref.⁶

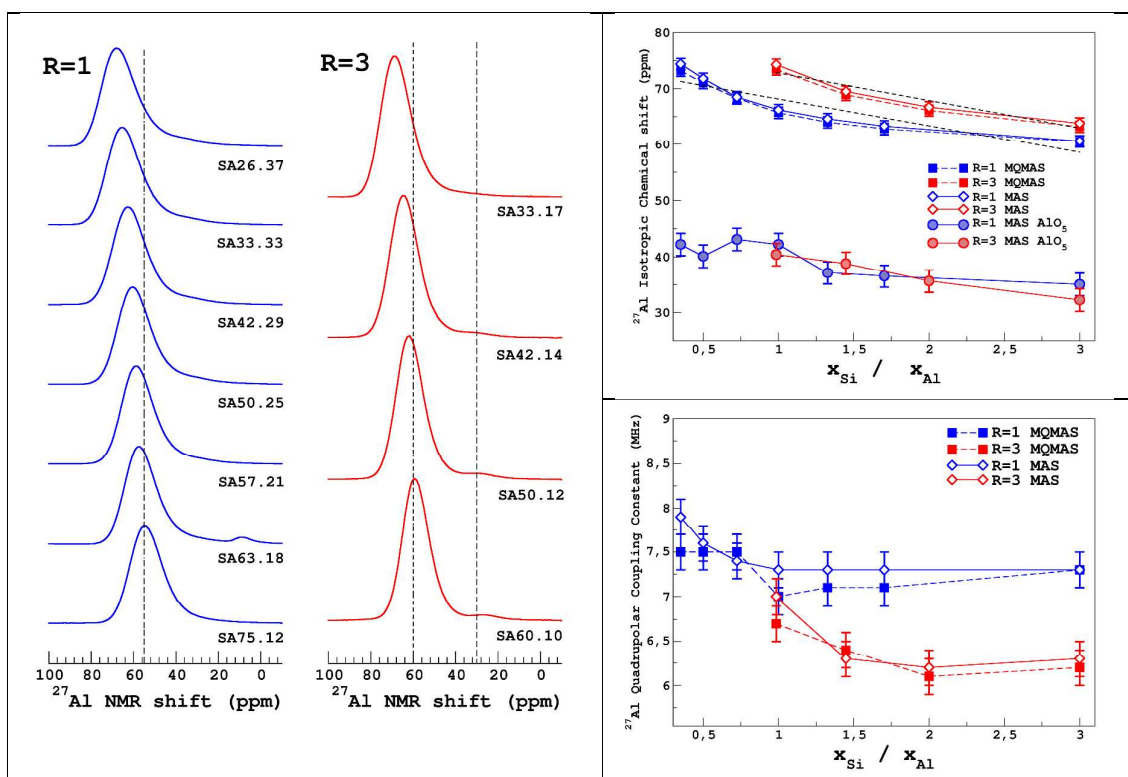


Figure 1. Left Panel: Experimental ^{27}Al MAS NMR spectra of the strontium aluminosilicate glasses. Right panel: Variation of the mean isotropic chemical shift (top) and quadrupolar coupling constant (bottom) values against the glass composition, for AlO_4 (and AlO_5 groups for isotropic chemical shift values only). Values obtained from the analysis of MAS and MQMAS spectra are compared. See Supporting Information for details.

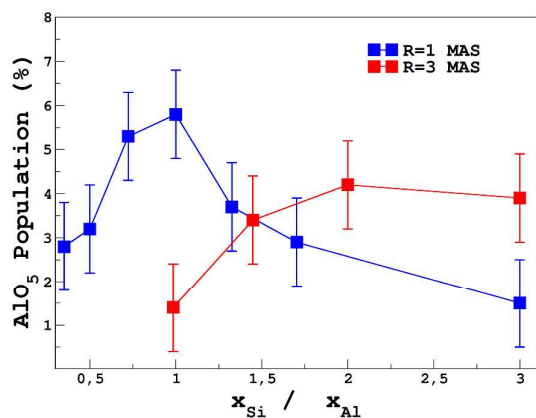


Figure 2. Variation of AlO_5 population against the glass composition.

Figure 3 shows the ^{29}Si MAS NMR spectra, the variations of the mean isotopic chemical shift δ_{iso} (i.e., center of gravity) and widths of the spectra; dashed lines represent linear regression of δ_{iso} values on specific ranges of composition (see below). For both glass series, increase of silica content yields a decrease of the isotropic chemical shift and increase of the spectrum's width. In the R = 1 glass series, according to previous studies of aluminosilicate glasses,^{9,53-55} the variation of δ_{iso} can be interpreted in terms of the Si/Al mixing. It has been generally observed that one substitution of one bonded silicon for an aluminum leads to shift between +3 and +5 ppm, in qualitative agreement with the observed slope of 2.1 ± 0.3 ppm/Al for the second part (for $x_{Al}/x_{Si} > 1.5$, i.e, SA50.25, SA57.21, SA63.18 and SA75.12) whereas the first part (for $x_{Al}/x_{Si} < 1.5$, i.e, SA26.37, SA33.33 and SA42.29) shows a slope of 12 ± 3 ppm/Al. This value approaches the R=3 glass series ones, with a higher slope for the increase of δ_{iso} , 18 ± 3 ppm/Al, which is clearly indicative of the contribution of two mechanisms : Al/Si mixing and decrease of the amount of non-bridging oxygens O^[1]. Each aluminum is coming with 1.5 Sr²⁺: the difference between the slopes, about 6 ppm/Al, can be ascribed to the effect of one added NBO in the case R=3. The residual of about 12 ppm/Al suggests that other mechanisms exist; MD can help understanding them.

In addition to the variation of δ_{iso} , both glass series show a significant increase of the spectra's widths against the silica content but with a similar slope. At first glance, this would suggest an increased local disorder around SiO₄ units for lower aluminum and strontium content. However, recent investigations of the dependence of the ^{29}Si isotropic chemical shift with the bond angle in tetrahedral linkages have shown that, depending on their connectivity, Q⁽ⁿ⁾ units may exhibit a different slope in their correlation between δ_{iso} and the average bond angle⁵⁶. In other words, Q⁽ⁿ⁾ units have a different NMR response to the local disorder so that they may be characterized by a different linewidth even for a similar bond-

angle distribution (BAD) around each environment. Such an effect will be investigated in a future work combining the present MD simulation with DFT-NMR calculations.

In conclusion, NMR clearly shows that tetrahedral coordination dominates the AlO_p speciations for all the glass compositions investigated and continuous and smooth Al/Si mixing occurs, as evidenced by the variations of the NMR parameters with the SiO_2 content. Additionally, the presence of a small amount of AlO_5 for all glass compositions suggest the presence of tricoordinated oxygens $\text{O}^{[3]}$ involved in the local charge balance, even for the $R = 3$ glass series.

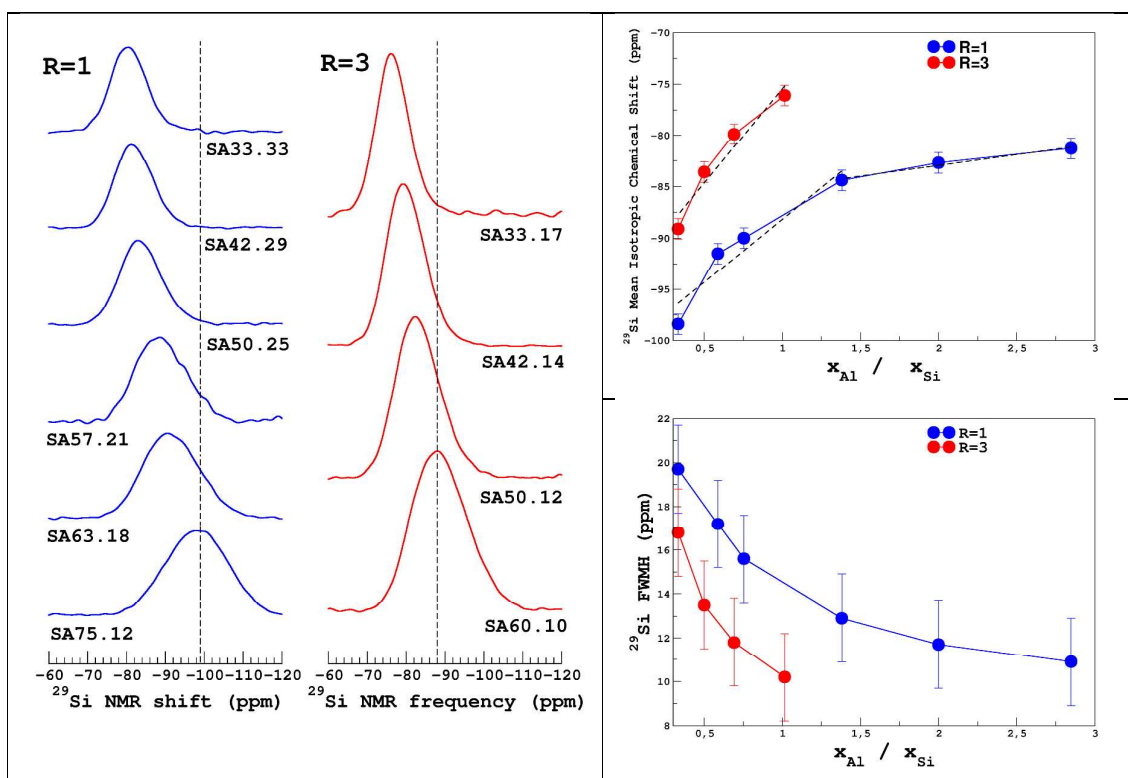
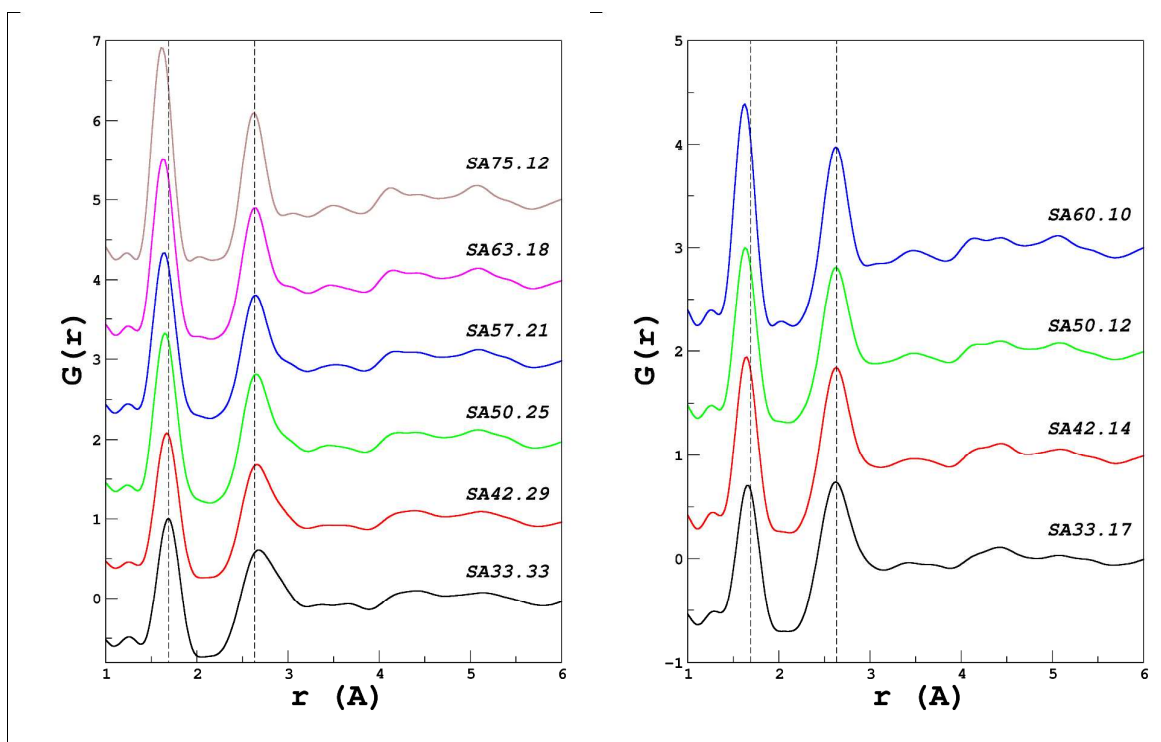


Figure 3. Left panel: Experimental ^{29}Si MAS NMR spectra of the strontium aluminosilicate glasses. Right panel: variation of the (mean) isotropic chemical shift (center of gravity, top) and the spectral width (full width at middle height, FWHM, bottom) against the glass composition.

3.2 Neutron Diffraction and Molecular Dynamics Simulations. Our glasses have been further characterized using neutron diffraction. Experimental data in reciprocal space could be well

reproduced by our MD simulations with the both potential models investigated in this work, as shown in the Supporting Information. Total structure factors were computed from partial structure factors using the standard approach based on the partial radial distribution function.²



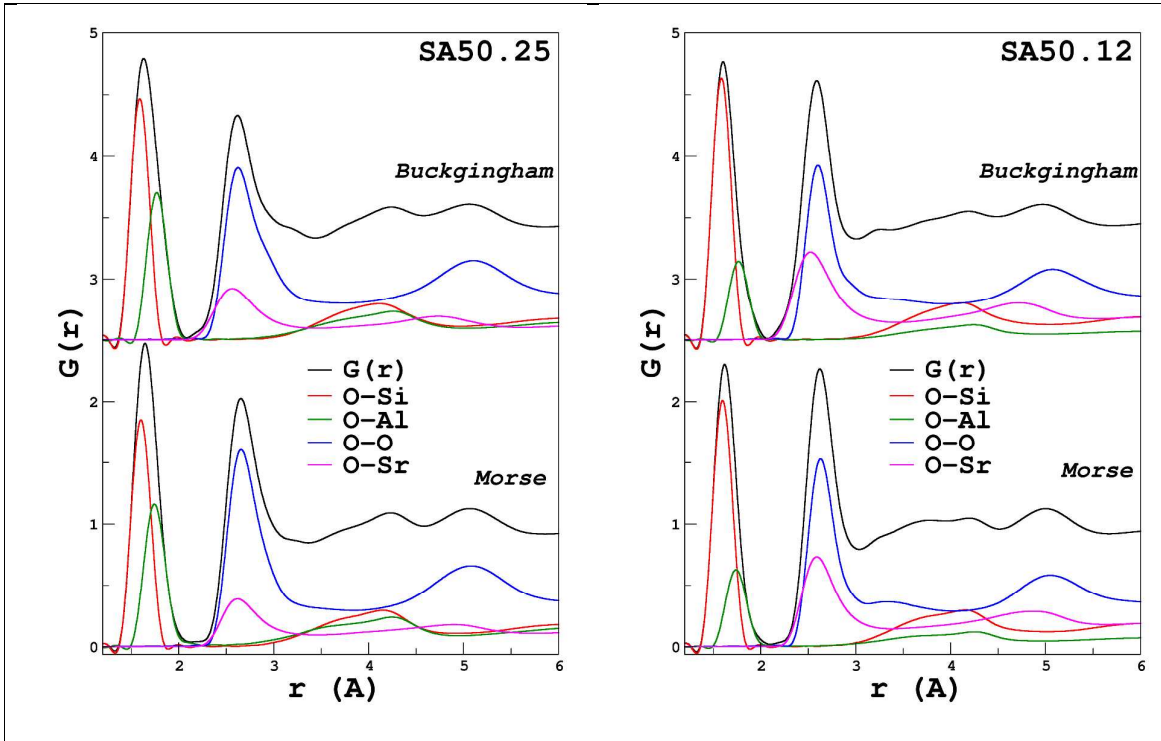


Figure 4. Upper panel, Total pair distribution function for the R=1 (left) and R=3 (right) glass series. Partial and total radial distribution functions obtained from MD simulations with Buckingham and Morse potentials for two representative glass compositions (accounting for finite- q acquisition in the reciprocal space).

3.2.1 Neutron data. As shown Figure 4, the strongest peak in experimental $g(r)$ centered at 1.7-1.6 Å shows a systematic shift with silica content. Partial contributions obtained from MD show that this peak is made up of the contribution of the Si-O pairs (1.60 Å) and the Al-O pairs (1.75 Å), in agreement with earlier computational and experimental studies.^{2-4,7,18,57-60} The position of the Si-O and Al-O peak is constant across the calculated compositional range, and changes in the first peak of $g(r)$ are therefore mainly reflective of the Si/Al variations in composition. The second peak of the radial distribution is located at around 2.6 Å and this peak is mainly a result of the O-O and Sr-O correlation centered at 2.65 Å and 2.44 Å, respectively. Further peaks are smoother and are the result of more complex mixtures involving mainly second neighborhood contributions O-X pairs and Si-Si pairs (at around 3.2 Å) are not analyzed here. It can be noticed that the broadening of the second peak in

experimental $G(r)$ (dashed lines at about 2.6 Å) for higher Al content can be ascribed, according to MD simulations, to O-(Al)-O distances. X-O bond lengths extracted from computed partial radial distribution functions (RDF), as generated by the MD simulations, are gathered in **Table 4**. The values are given for two representative glass compositions together with averaged values over all glass compositions of each glass series. Because of the non-negligible influence of the atomic speciation on the bond lengths, it was systematically taken into account (but only non-negligible populations are given).

Table 4. Bond Lengths extracted from Partial RDFs (Peak Maximum and in parentheses Half Width at the Middle Height) for Two Representative Compositions (SA50.25 R=1 and SA50.12 R=3) and Averaged Values over all Glass Compositions (Buck. is the Buckingham model)

Bond length (Å)	SA50.25		SA50.12		Average R=1		Average R=3	
	Buck.	Morse	Buck.	Morse	Buck.	Morse	Buck.	Morse
Si-O ^[2]	1.60 (0.04)	1.62 (0.05)	1.61 (0.04)	1.62 (0.05)	1.60 (0.04)	1.62 (0.05)	1.61 (0.04)	1.62 (0.05)
Si-O ^[1]	1.57 (0.03)	1.58 (0.04)	1.57 (0.03)	1.58 (0.04)	1.57 (0.03)	1.58 (0.04)	1.57 (0.03)	1.58 (0.04)
Al ^{IV} -O	1.79 (0.06)	1.76 (0.07)	1.78 (0.05)	1.76 (0.06)	1.79 (0.06)	1.76 (0.07)	1.78 (0.05)	1.76 (0.06)
Al ^V -O	1.89 (0.11)	1.89 (0.13)	1.90 (0.10)	1.89 (0.12)	1.90 (0.11)	1.89 (0.13)	1.90 (0.10)	1.89 (0.12)
Sr-O ^[2]	2.83 (0.31)	2.92 (0.29)	2.90 (0.31)	2.94 (0.29)	2.84 (0.31)	2.91 (0.29)	2.89 (0.31)	2.93 (0.29)
Sr-O ^[1]	2.56 (0.24)	2.67 (0.23)	2.62 (0.27)	2.71 (0.25)	2.54 (0.24)	2.67 (0.23)	2.62 (0.27)	2.71 (0.25)

As already noticed in previous MD studies⁶¹⁻⁶³, Si-O^[1] bonds are shorter by about 0.03-0.04 Å with respect Si-O^[2] (O^[2] represents bridging oxygens) bonds; the Morse potential predicts slightly longer distance (0.01-0.02 Å) than Buckingham. Concerning aluminum, Al^V-O distance exceeds Al^{IV}-O one by about 0.1 Å for Buckingham and 0.12 Å for Morse model. As detailed in the Supporting Information, the larger dispersion in Al^V-O bond lengths is a consequence of the fact that in most cases, among the five bond lengths, two bonds were found to be systematically much longer than the three shorter ones, which turn out to be rather close

Al^{IV}-O distances. Bond lengths for Si-O^[2], Si-O^[1], Al^V-O and Al^{IV}-O were found to be - on average - quite constant across all studied compositions for both potential sets. This contrasts the behavior of Sr-O distances which show strong variations with composition as detailed in the Supporting Information and quite significant differences are observed between the two potentials sets (**Table 4**). Sr-O^[2] and Sr-O^[1] distances are longer for the Morse potential sets versus Buckingham ones, with differences in between 0.1 and 0.15 Å. In these respects, Buckingham potential sets seems to favor Sr-O interactions (and particularly Sr-O^[1]) with respect to the Morse potentials sets. Larger dispersion values are observed for Sr-O distances and highlights the fact the first coordination sphere of Sr is less well-defined (*vide infra*) as generally observed for alkali and alkaline-earth.^{4,62} As will be seen later, this pronounced difference between the two potential sets results in rather different population oxygen species O^[1-3], but also on strontium coordination numbers, as discussed in the next section.

3.2.2 Oxygen environment. Variations of the oxygen speciation populations are summarized in Figure 5. For R=1 compositions, both models show a non-negligible amount of O^[1] (NBO) and O^[3] (TBO) which concentration decreases with the Si content. At high aluminum content, the Morse potential sets shows a much higher concentration of O^[1] and O^[3] (~20%) than Buckingham (~10%). Globally, if more depolymerized structures are predicted with the Morse potential sets (in terms of O^[1] concentration), they also contain a much higher content of O^[3]. The presence of a non-negligible amount of O^[1] in tectosilicate compositions has been experimentally observed for several other glass compositions,^{13,14,64} requiring the formation of other species such as AlO₅ (see below) or O^[3] to maintain the local charge balance.

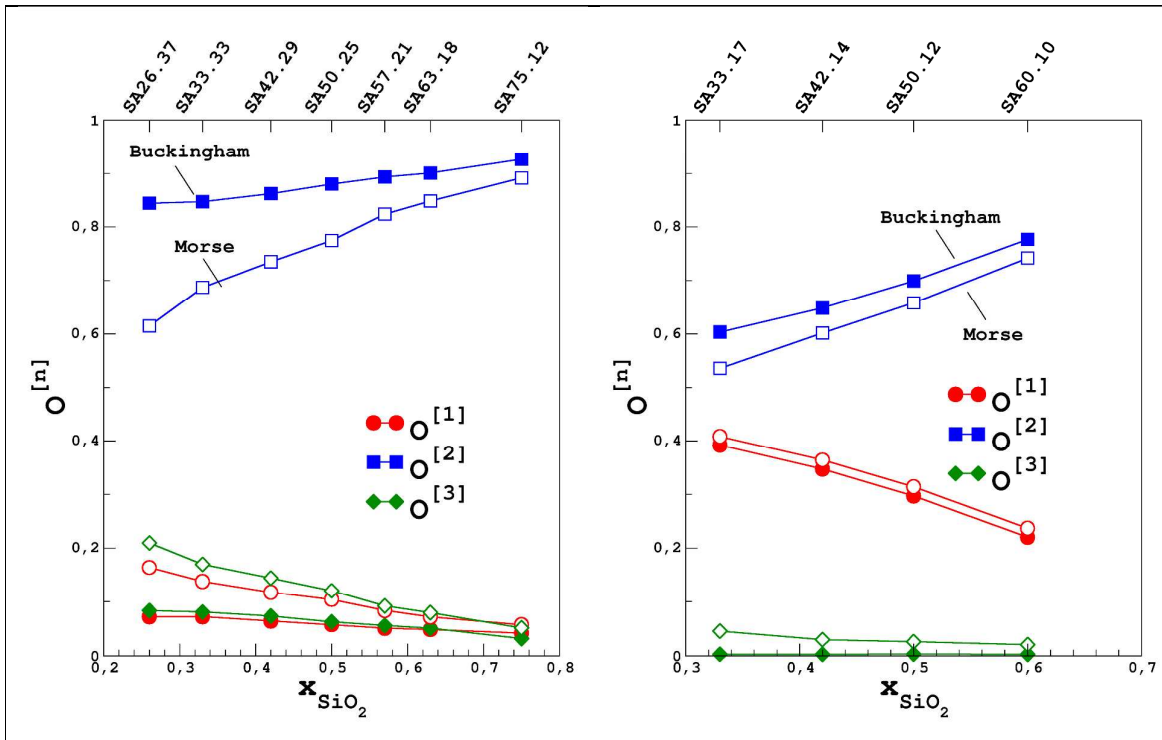


Figure 5. Variations of the oxygen speciation populations with the glass compositions predicted with the two potential models studied. (Closed symbols: Buckingham; Open symbols: Morse).

For $R = 3$, if nearly identical $O^{[1]}$ populations are predicted for both models, only the Morse potential predicts $O^{[3]}$ (~5%) resulting in a lowering of the $O^{[2]}$ concentration by 5-10% as compared with Buckingham model. As expected $O^{[1]}$ population decreases linearly with the silica content (or equivalently increases with the SrO content).

3.2.3 Aluminum environment. Variations of the Al speciation populations (AlO_4 , AlO_5 and AlO_6) are displayed in Figure 6. For $R=1$ compositions, tetrahedral Al is dominant with a nearly constant concentration of 5% AlO_5 for the Buckingham potential, in good agreement with NMR experiments, whereas Morse Potential sets predict much higher AlO_5 population which decreases with the silica content (in addition to a small fraction of AlO_6 following the same trend). At high silica content, both models become equivalent. No noticeable population of NBO on the AlO_4 nor the AlO_5 or AlO_6 units is observed, in agreement with Al-

NBO being energetically less favorable than Si-O^[1] bonds.^{1,64} For R=3 compositions, a dominant AlO₄ population is predicted but with a nearly constant AlO₅ population: 10% for the Morse model and 5% for the Buckingham model, both in quite good qualitative agreement with the NMR experiments. In this respect, MD simulations corroborate the presence of AlO₅, even with a large excess of SrO.

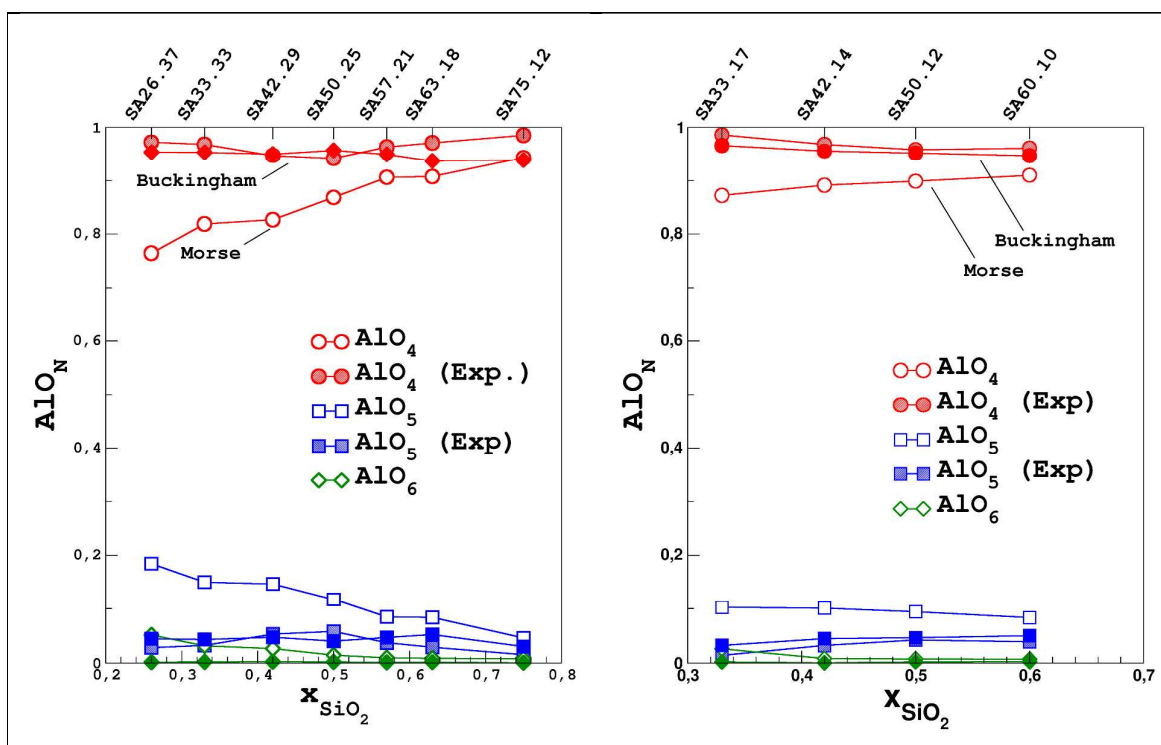


Figure 6. Variations of the Al speciation populations (AlO_p) with the glass composition for the two potential sets studied. (Closed symbols: Buckingham; Open symbols: Morse).

O-Al-O bond angle distributions are displayed in Figure 7 for two representative glass compositions. Four-folded Al are in rather regular tetrahedral units showing a narrow distribution of O-Al-O angles centered around 109.5°. For 5-folded atoms, a broader O-Al-O angle distribution is observed with the main peak at 90° followed a very broad peak a 170°. This is indicative of a bipyramidal rather than a squared based pyramid geometry. The two

potentials yield close O-Al-O bond angle distribution (BAD); with a slightly broader peak at 90° for AlO₅ for the Morse potential, reflective of more distorted units.

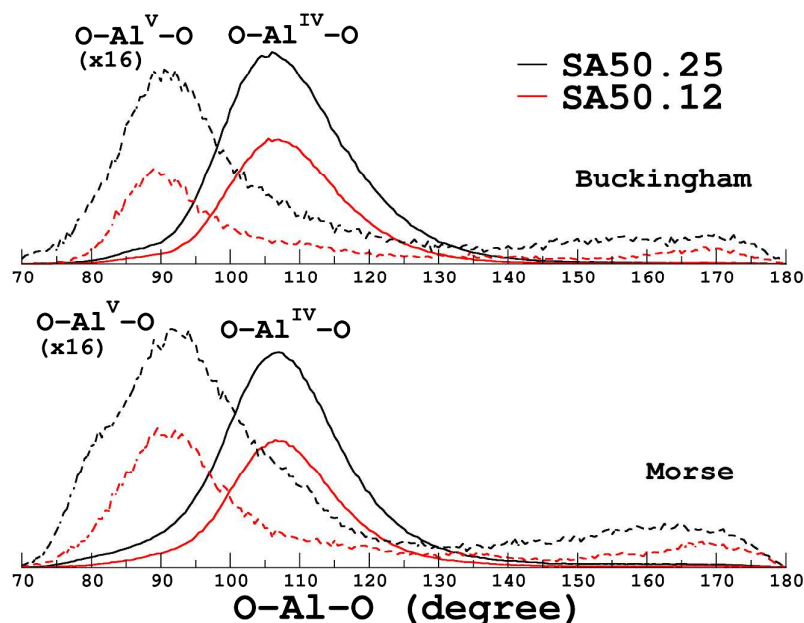


Figure 7. O-Al^{IV}-O and O-Al^V-O Bond Angle distribution for two representative glass compositions.

Figure 5 and Figure 6 suggest that the amount of AlO₅ units correlate to the amount of O^[1] and O^[3]. For Morse potentials, were the AlO₅ fraction span a wider range of values, O^{[1],[3]} populations are indeed found to correlate to AlO₅ fraction (see Supporting Information). This point will be further discussed below in connection with the presence of small rings.

3.2.4 Silicon environment. O-Si-O bond angle distributions (shown Supporting Information) show that for both potential sets silicon tetrahedral units are well ordered with a narrow distribution around 109.5° (100% of the silicon atoms are in tetrahedral units). The variations of the Q⁽ⁿ⁾ units with glass compositions are displayed in Figure 8; note that only Q⁽²⁾, Q⁽³⁾ and Q⁽⁴⁾ units are present.

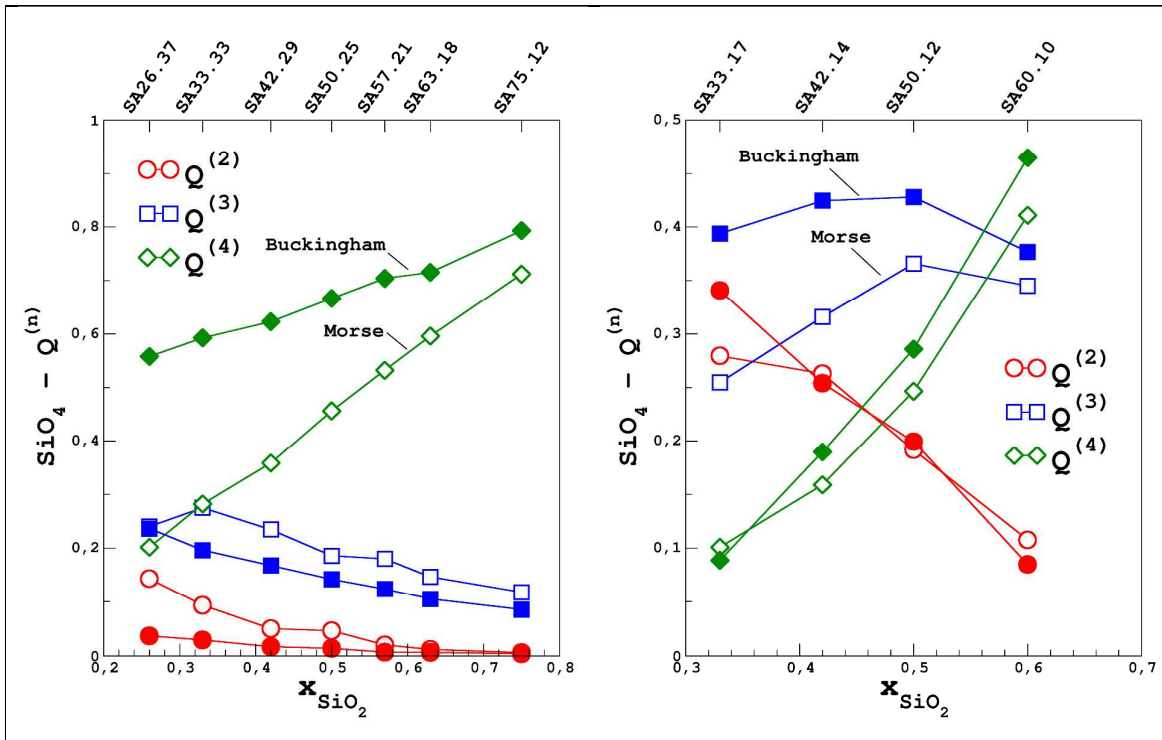


Figure 8. Variations of the $Q^{(n)}$ fractions with the glass composition (Left $R=1$ and right $R=3$ glass series). (Closed symbols: Buckingham; Open symbols: Morse).

For $R = 1$ compositions, despite the exact charge balance condition, a significant fraction of Si tetrahedral units are disconnected from the network ($O^{[1]}$) with a marked difference between the two potential sets in term of the $Q^{(4)}$ units. As expected from the oxygen speciation analysis (Figure 5), the Morse potential sets predict a much less polymerized network, but both exhibit a global increase $Q^{(4)}$ with silica content. For low silicon content (< 50%), the Buckingham model favors a bimodal distribution of $Q^{(n)}$ units ($Q^{(3)}$ and $Q^{(4)}$) whereas a trimodal distribution is predicted for the Morse model, with $Q^{(2)}$ units. For high silicon content, both models converge to a bimodal distribution of $Q^{(3)}$ and $Q^{(4)}$ units.

For $R=3$ compositions, $Q^{(3)}$ units are the most frequent with a concentration ranging from 30 to 40%. The linear increase of $Q^{(4)}$ at the expense of the $Q^{(2)}$ units with the silica content is similar for both potential sets.

3.2.5 Strontium environment. Comparison between the Sr-BO and Sr-NBO partial RDF for the two potential sets is displayed in Figure 9 for two representative glass compositions. The decay of the partial Sr-NBO RDF to zero and its smaller width (than Sr-BO) reveal that the environment of strontium atoms is better defined when accounting for the NBOs only. The O-Sr-O angle distributions show standard shapes for modifier cations (see Supporting Information), characterized by a broad distribution covering the range 40°-180° with peak maxima at 50°, 80° 110°, thus reflective of the variety of Sr polyhedral types, as also illustrated by the broad distribution of the coordination numbers (CN) displayed in Figure 9 (right panel). A large dispersion of CNs is observed with values ranging from 6 to 10 (with max CN at ~7-8). Such high CN values can be understood considering the relatively medium cation field strength (CFS) of strontium and our simulations are in agreement with previous MD studies of more complex glass compositions.^{59,65,66} A more detailed analysis of CNs (Figure 10) shows that for R = 1 strontium environment is dominated by bridging oxygen atoms, in agreement with the low amount of O^[1] expected in this system, whereas for R=3 the first coordination sphere is almost equally shared by O^[1] and O^[2] atoms. This first coordination analysis underlines that Sr atoms (but this also applies to any modifier cation) cannot be unambiguously classified as network modifier nor charge compensator solely; its structural role is more likely to be in between, depending upon the relative contribution of O^[1] and O^[2] atom to its CN value (note that Sr sees only few O^[3]).

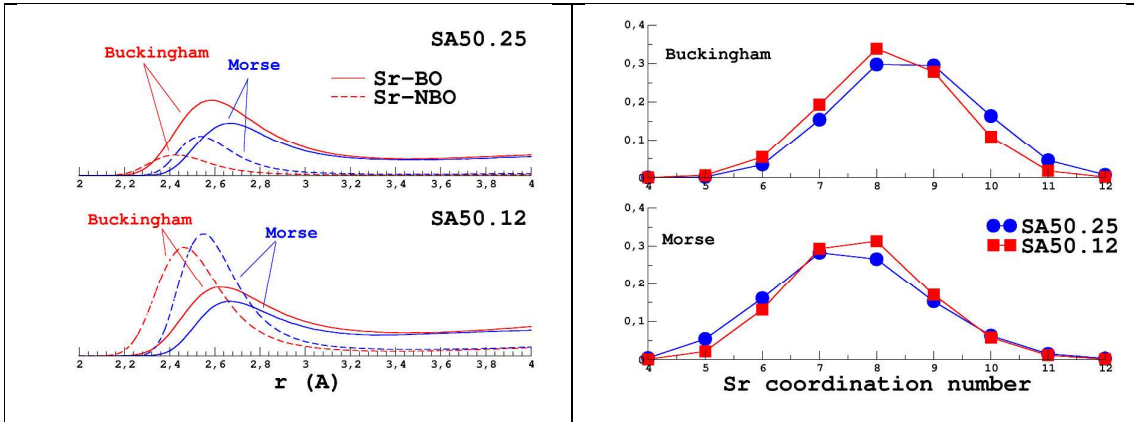


Figure 9. Left panel: example of decomposition of the Sr-O partial radial distribution function into Sr-O^[1] and Sr-O^[2] contributions for two representative compositions as obtained in MD simulations. Right panel: distribution of strontium coordination numbers.

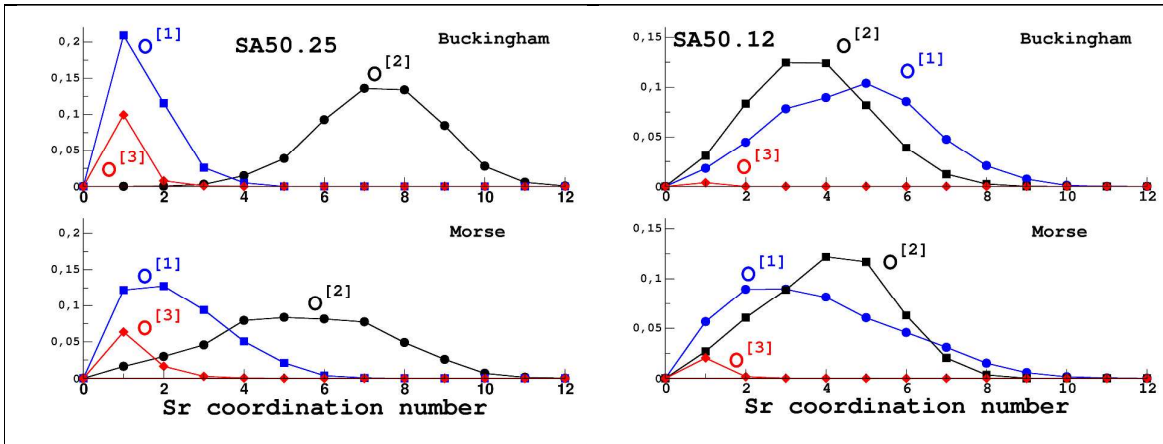


Figure 10. Decomposition of the strontium coordination number distributions for two glass compositions in terms of non-bridging oxygen (O^[1]), bridging-oxygen (O^[2]) and tri-coordinated oxygen atoms (O^[3]).

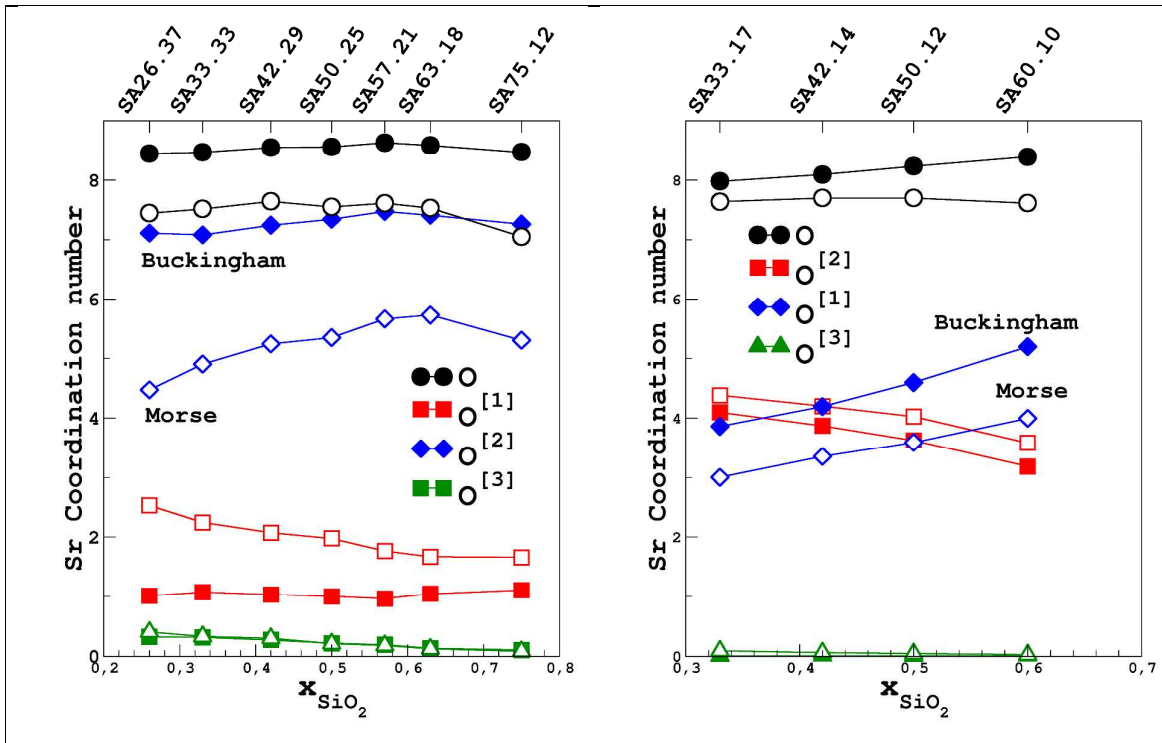


Figure 11. Variation of the averaged strontium coordination numbers with the glass composition (Closed symbols: Buckingham; Open symbols: Morse).

For all glass compositions, the decomposition of the average CN_0 in terms of bridging ($O^{[2]}$), non-bridging ($O^{[1]}$) and tricoordinated ($O^{[3]}$) oxygen atoms are shown in Figure 11. For the $R = 1$ glass series, CN_0 is rather constant ($\sim 7-8$) with a difference of about 1 between the two potential sets. This difference is more pronounced (almost 2) when considering bridging-oxygen only but partially compensated by an inverted trend for $O^{[1]}$ showing a difference between -0.5 and -1. Thus, the Morse potential sets favor Sr- $O^{[1]}$ contacts compared to the Buckingham potential sets. This leads to a higher number of coordinated $O^{[2]}$ (and globally of oxygen) for the latter model. In contrast, both models have a similar trend in terms of $O^{[3]}$ with a value varying from 0.4 to 0.1 with silica content increasing.

Similar differences between both potential sets are observed for the $R=3$ glass series but are less pronounced. As expected from the dominant modifier role of strontium for $R=3$, contribution of $O^{[1]}$ is much higher (~ 4) but also quite close to $O^{[2]}$ which is in turn much

lower (~4-5) than for R=1 glasses. This yields a global coordination number CN_O of 8, very close to the R=1 glass series value. This number is nearly constant as a result of an increase of $O^{[2]}$ contribution which is partially compensated by a decrease of $O^{[1]}$.

These results suggests that the presence of $O^{[3]}$ units is not correlated to Sr-O interactions (which differs between the two potential models) but more likely related to Al-O interactions: Sr-O bond lengths are rather similar for the two potential sets (**Table 4**). Experimentally, presence of $O^{[3]}$ is expected based on the presence AlO_5 units as observed by NMR (Figure 2). Spatial distribution of $O^{[3]}$ within the simulation cell and their exact contribution to global charge compensation mechanisms will be investigated in a future work with the help of quantum chemical calculations.

In order to further analyze the Sr-O contacts independently of populations of the various oxygen speciations which have to be shown to be governed by the short-range potential models we introduce a preference factor P which accounts for the *preferential* contact of strontium cations with $O^{[q]}$ atoms. The latter is defined^{51,67,68} as

$$P = \frac{N_q^p}{p \times xO^{[q]}} \quad (4)$$

where N_q^p is the number of coordinating oxygen $O^{[q]}$ of SrO_p clusters and $xO^{[q]}$ is the fraction of $O^{[q]}$. $P > 1$ means preferential interaction. The results of this analysis are shown in Figure 12 for the most abundant SrO_p clusters ($p = 7$ for Morse and $p = 8$ for Buckingham potential sets). Both potential sets give the same results for $O^{[2]}$ and $O^{[1]}$ whereas Sr- $O^{[3]}$ contacts are more favored with the Buckingham potential sets.

For R=1, a strong preference for $O^{[1]}$ is noticed, increasing with silicon content, whereas interaction with $O^{[2]}$ is almost constant and close to 1, i.e. $O^{[2]}$ are more likely to be randomly

distributed around the strontium atoms. This behavior can be explained by the low content of $O^{[1]}$ atoms which need to be charge compensated; the $O^{[1]}$ concentration decrease with silica content manifests itself by an increase of the $O^{[1]}$ preference factor. $Sr-O^{[3]}$ contacts are unfavored and nearly constant with the glass composition. For the R=3 glasses, the higher strontium concentration results in a lower preference factor for NBO (but still > 1), also increasing with silica content, and to slightly unfavored $Sr-O^{[2]}$ contacts (but still close to random).

In conclusion, this analysis demonstrates that both potential sets yield similar behavior of preference factors for $Sr-O^{[2]}$ and $Sr-O^{[1]}$ contacts. This suggests that they are somewhat independent of the short repulsion terms, and most likely to be governed by Coulombic interactions. $O^{[2]}$ are distributed almost randomly around the strontium atoms. The observed differences in $CN_{O[2]}$ and $CN_{O[1]}$ (Figure 11) seem to be therefore *first* a consequence of the global population of $O^{[2]}$ and $O^{[1]}$ which in turn depends on the chosen potential sets.

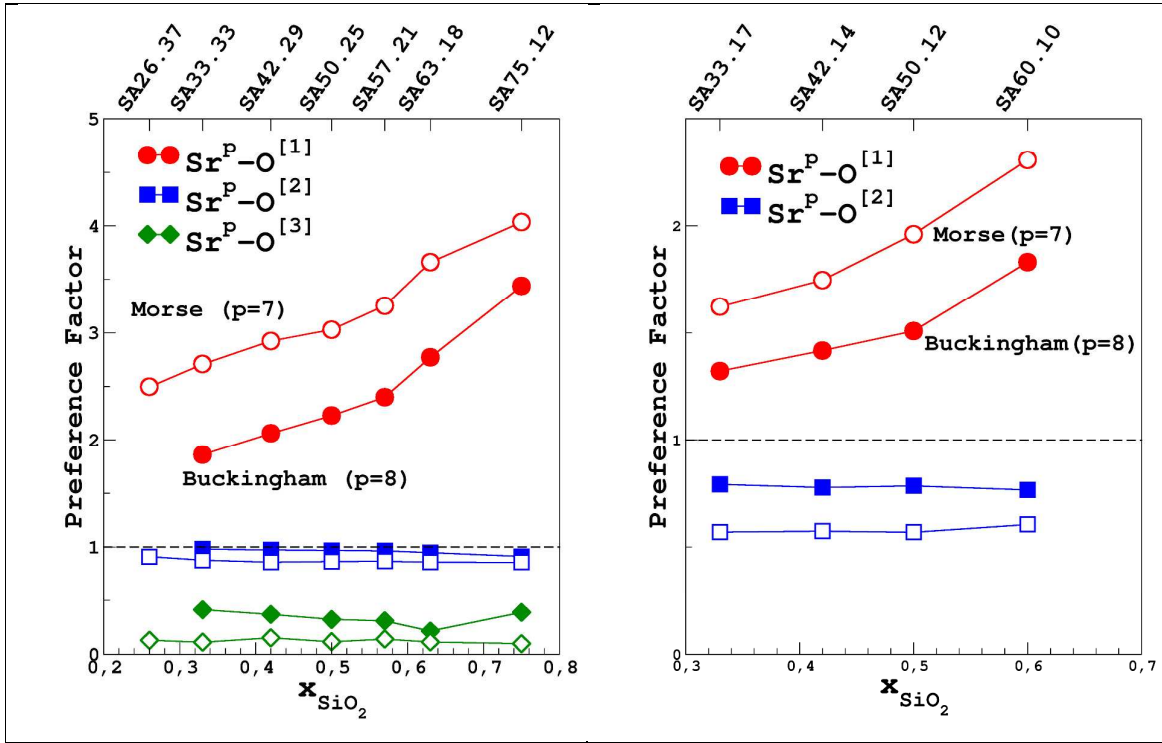


Figure 12. Variation of the preference factor P (Eq. (4)) with the glass composition for the most populated SrO_p cluster (Closed symbols: Buckingham; Open symbols: Morse). Left $R=1$ and right $R=3$ glass series.

3.2.6 Al/Si mixing. To investigate the Al/Si mixing, $\text{T-O}^{[2]}-\text{T}'$ ($\text{T}, \text{T}' = \text{Al}, \text{Si}$) relative populations have been calculated and are displayed Figure 13. They vary in a similar way for both models across the calculated compositional range. It is important to note that the populations displayed corresponds to the conditional probabilities $p(\text{T}-\text{O}-\text{T}' | \text{O} = \text{O}^{[2]})$; in other words, this means that the dependence upon the total population of bridging oxygens, i.e., $p(\text{O}^{[2]})$ (see Figure 5) has been compensated. For a comparison, variations of the *total* fraction of $\text{T-O}^{[2]}-\text{T}'$, that is $p(\text{T}-\text{O}-\text{T}') = p(\text{T}-\text{O}-\text{T}' | \text{O} = \text{O}^{[2]}) \times p(\text{O}^{[2]})$ are given in the Supporting Information.

Figure 13 highlights the fact the pairing of Al/Si is independent on the potential sets chosen, even of the fractions of $\text{O}^{[n]}$ ($n=1, 2, 3$) species are strongly dependent on it. This suggests that Al/Si are mainly governed by electrostatic (here, Coulombic) interactions. Comparison with a binomial model (dashed lines in Figure 13) indicates that the Al/Si mixing on bridging

oxygen possess some ordering characteristics when aluminum is involved whereas Si-O-Si population follows closely the binomial model. Si-O-Al linkages are clearly favored in contrast to Al-O-Al ones, a fact which has been often observed experimentally.^{1,13,69,70}

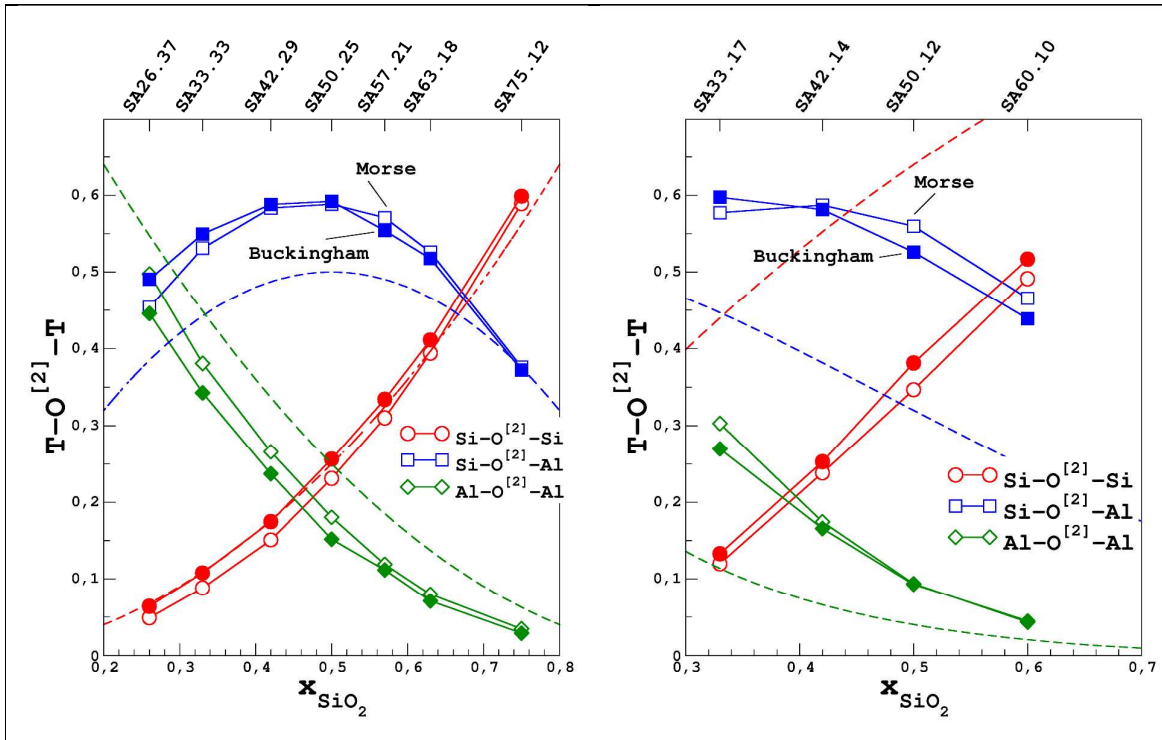


Figure 13. Variations of the $T-O^{[2]}-T$ relative populations ($T=Al, Si$) with the glass compositions predicted by the two potential models studied. Dashed represents random probabilities calculated from the glass composition (i.e., binomial law).

Variations of $O^{[1]}-T$ reveals that in both models, $O^{[1]}$ predominantly bounds to Si, in agreement with experimental NMR observation (Figure 14). $O^{[3]}$ population analysis confirms that OAl_3 and OAl_2Si are the most favorable configurations (Figure 15).

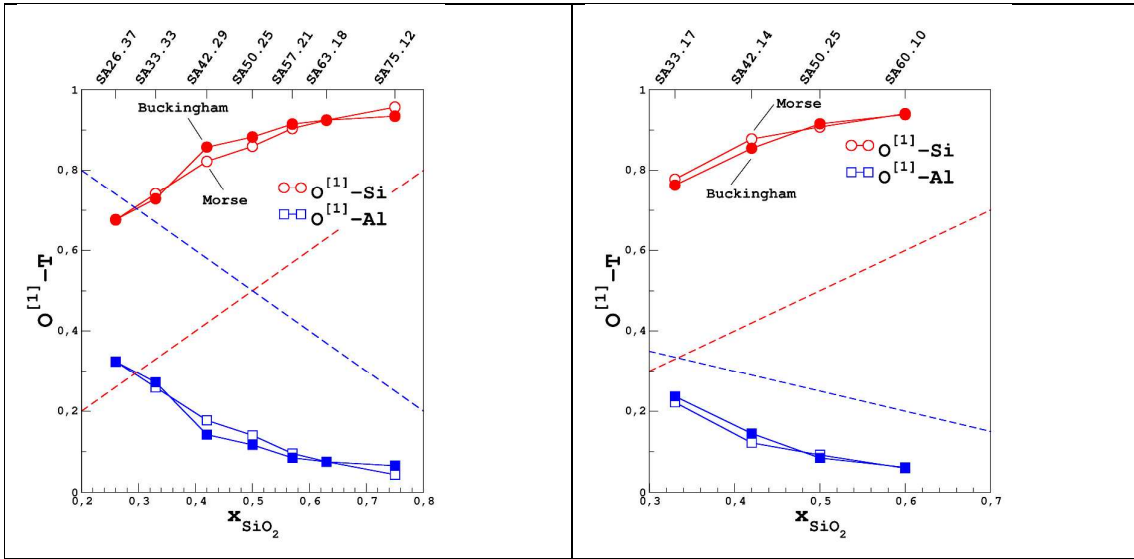


Figure 14: Variation of (left and middle panel) the $O^{[1]}-T$ populations ($T=Al, Si$) with glass composition for the two potential sets studied. Dashed lines represents random probabilities calculated from the glass composition.

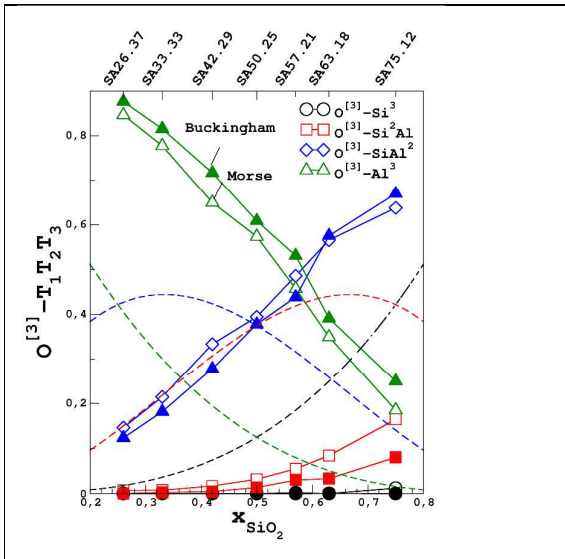


Figure 15. Variation of $O^{[3]}$ with glass composition for the two potential sets studied. Dashed lines represents probabilities calculated from the glass composition (i.e. random bonding to Al or Si atoms).

3.2.7 Bond angle distribution and primary ring structure. Bond angle distributions SiOSi, SiOAl and AlOAl are plotted in Figure 16 for two representative glass compositions from the R=1 and R=3 glass series. Left panel shows that both potential models produce similar shape. For BO, the BAD extend from 120° to 180° with peak maxima at $140-150^\circ$ in the order

SiOSi>SiOAl>AlOAl, they are standard values in aluminosilicate glasses. In the case of O^[3], Al-O^[3]-Si BAD shows a narrower distribution with peak maxima at 120° whereas Al-O^[3]-Al has two maxima at 120° and 90°. Right panel reveals that no clear correlation of the bond angle with the coordination number of the oxygen atom can be established, in contrast to other cations.⁷¹

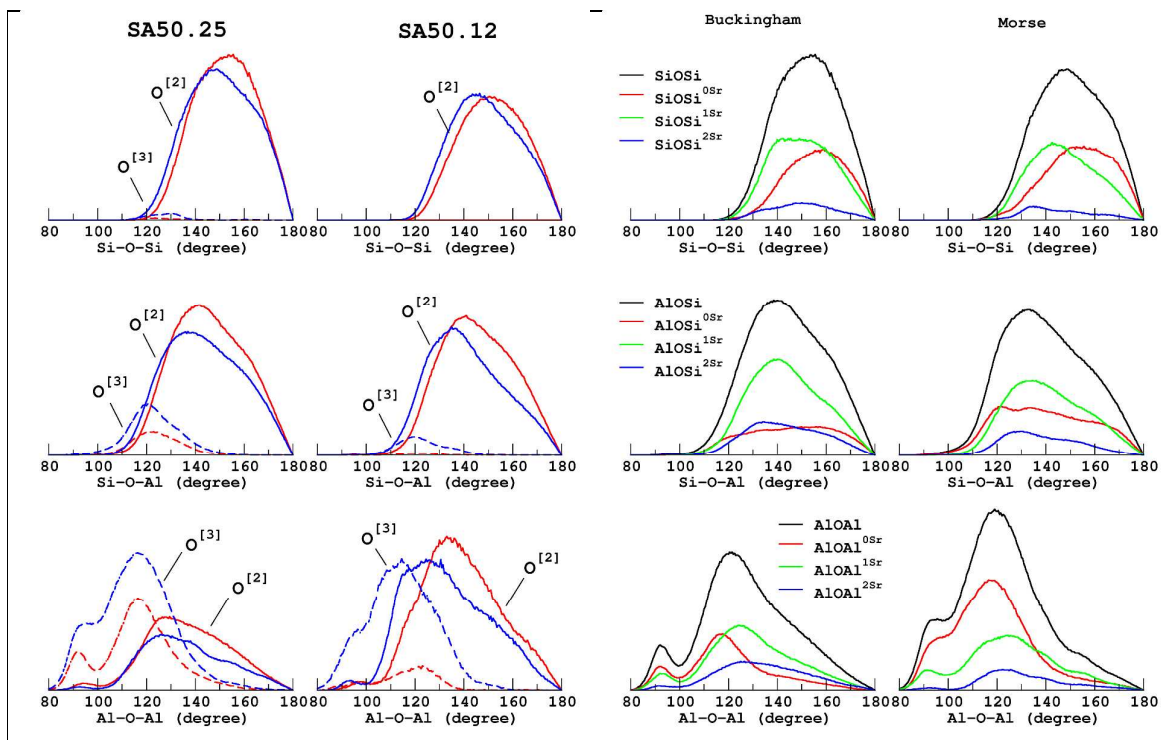


Figure 16. Left panel: SiOSi, SiOAl and AlOAl bond angle distributions (BAD) for two representative glass compositions for the two potential sets (blue lines: Morse and red lines: Buckingham). Right panel: For SA50.25 glass, analysis of the BAD in terms of the strontium coordination number of the oxygen (Buckingham potential sets). TOT^{NSr} (T=Si or Al) represents the BAD for oxygen atoms coordinated by N strontium atoms.

To establish whether a correlation exists between ring size and coordination number of aluminum (AlO_{5,6}) or tricoordinated oxygen (O^[3]), a primary ring search has been performed by shortest-path analysis. For silicon SiO₄, aluminum AlO_{4,5} and oxygen O^{[2],[3]} atoms, Figure 17 and Figure 18 show the fraction of each units considered in a given primary ring size.

For SiO_4 units, across all compositions ($R=1$ and $R=3$), 8-fold rings dominates with an opening of the structure for higher silica content: the 10-fold ring population increases at the expense of the 6-fold rings. For AlO_4 units, a similar behavior is observed between the two glass series but with higher population of 6-fold rings and about 10% of the AlO_4 are involved in edge-sharing (4-fold ring) configurations. In the case of AlO_5 for the $R=1$ compositions, higher coordination states are primarily involved in edge-sharing configurations (approx. 70%) and in 6-fold rings (approx. 20%). For the $R=3$ glass series, the two potential sets exhibit significant differences: Morse model strongly favors edge-sharing configurations whereas Buckingham model favors 6 and 8-fold rings.

Concerning the oxygen (Figure 18), bridging oxygens $\text{O}^{[2]}$ are mainly involved in 8 to 10-fold rings, with 6-fold rings decreasing with the silica content. This trend is observed for the two glass series. This confirms that at higher aluminum content a more connected network is predicted. $\text{O}^{[3]}$ are equally shared between 4 and 6-fold rings (6 and 8-fold rings, respectively) for the $R=1$ compositions ($R=3$, respectively), with slight differences between the two potential models.

This analysis suggests that AlO_5 together with $\text{O}^{[3]}$ are mainly responsible for the formation of small ring structures, especially the formation of edge-sharing configurations and, to a lesser extent, of six-membered rings. A quantitative analysis of the charge distribution would be of interest to decipher their exact contribution to the global and local charge balance mechanisms, especially for the $R=1$ compositions. As requiring more sophisticated methods to be employed such as DFT calculations and ab-initio molecular dynamics, such a work is in progress and will be presented elsewhere.

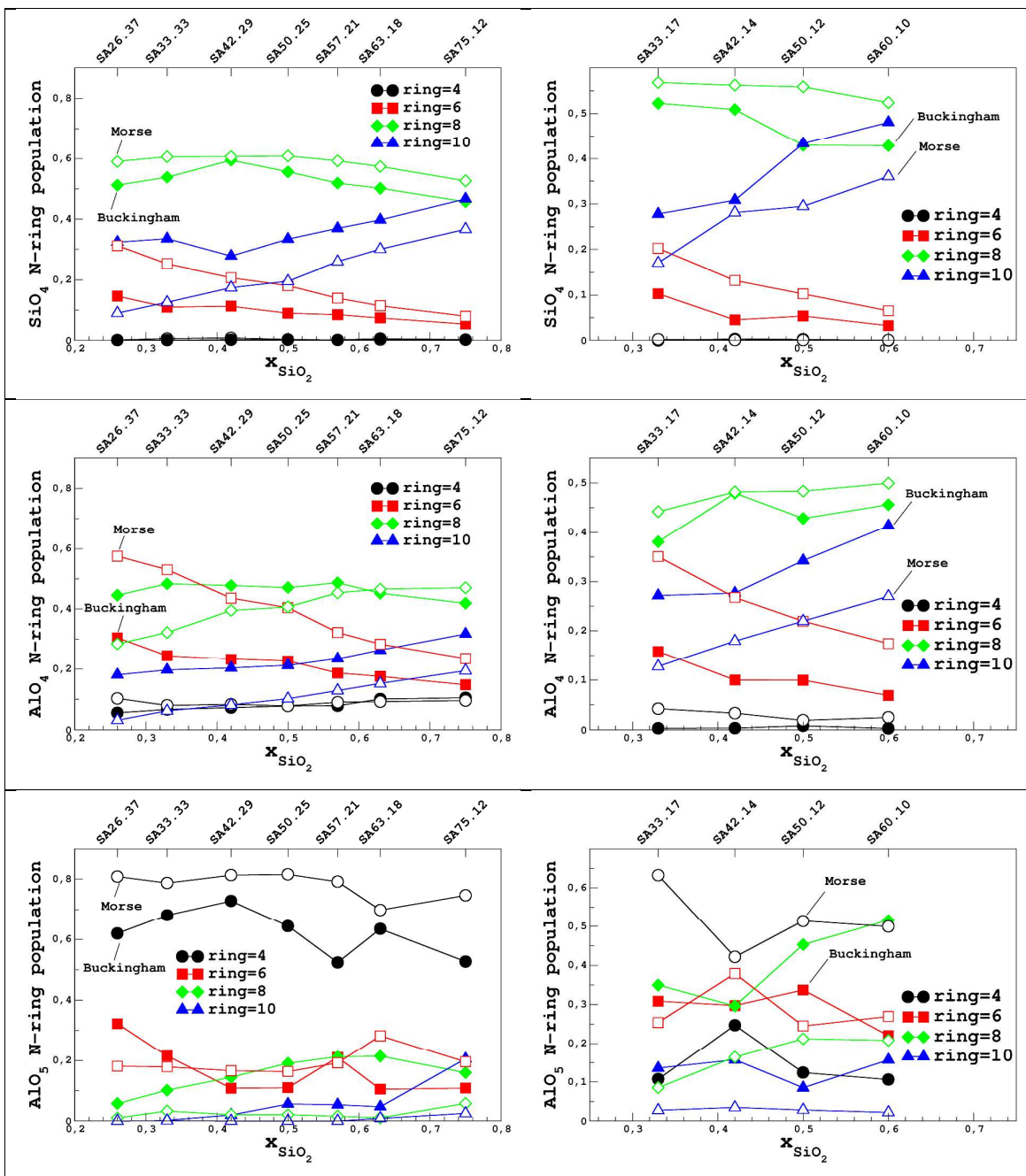


Figure 17. Variations with the glass composition of the ring size populations for tetrahedral silicon (top), tetrahedral aluminum (middle) and five-fold coordinated aluminum (bottom). Only small ring-sizes (which are also the most populated) are shown. Open and filled symbols for the Morse and Buckingham potential sets, respectively.

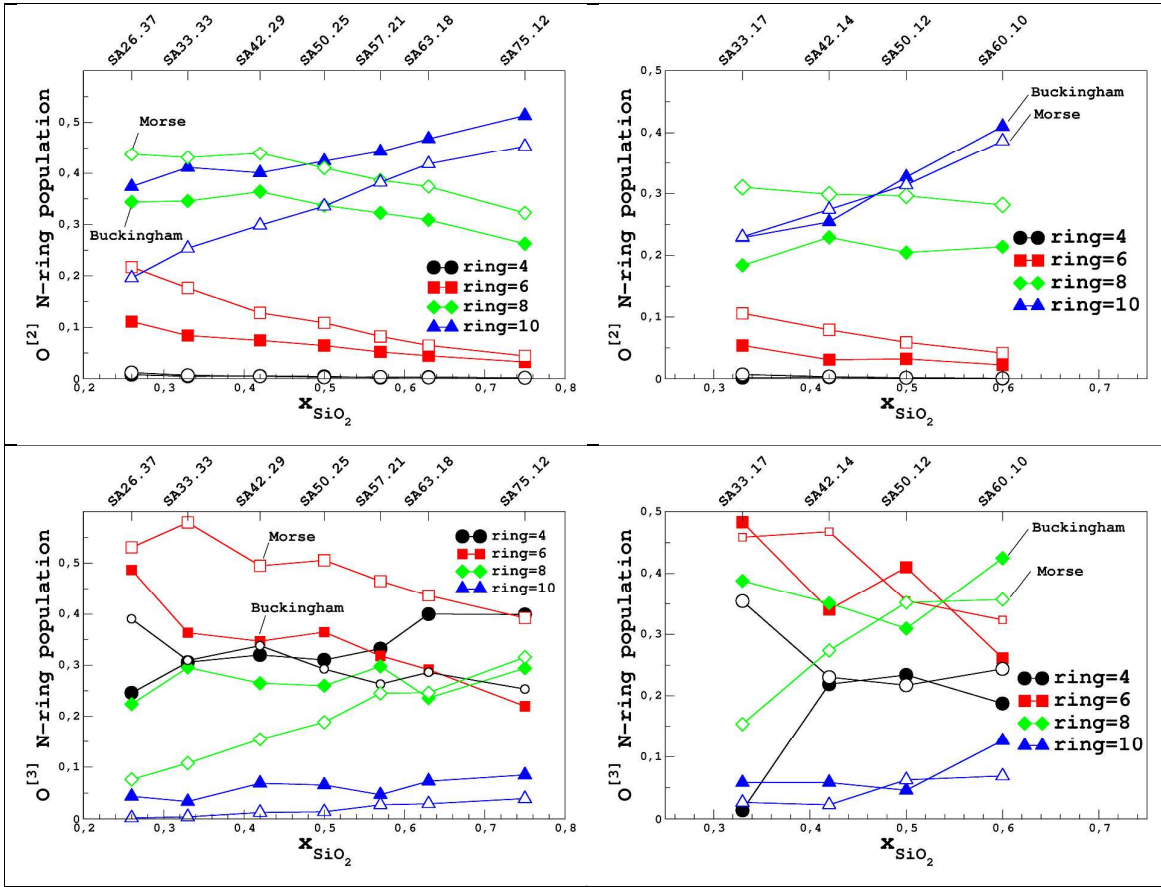


Figure 18. Variations with the glass composition of the ring-sizes of oxygen species: bridging-oxygen $O^{[2]}$ (upper) and tri-coordinated oxygen $O^{[3]}$ (lower) atoms. Open and filled symbols for the Morse and Buckingham potential sets, respectively.

4. Conclusion

Molecular dynamics simulations have been performed to investigate the structure of strontium aluminosilicate glasses. Two popular potential forms are compared for the short-range interactions: the Morse and Buckingham forms. For both models, a good agreement is obtained with the neutron diffraction data and NMR experiments: aluminum is predominantly in tetrahedral form with a small amount (few %) of fivefold units, as previously experimentally observed in calcium aluminate silicate glasses.¹⁰ A continuous decrease of ^{27}Al isotropic chemical shift in AlO_4 units with the Si/Al ratio is observed, mostly dictated by the Al/Si mixing and in agreement with previous NMR studies in aluminosilicates. Similarly, ^{29}Si isotropic chemical shifts increases with the Al/Si ratio with a slope in

agreement with observed values reported in literature. O-Al and O-Si interatomic distances are found to be constant across the calculated compositional range and close to values determined in the extensively investigated calcium aluminosilicate glasses. Sr-O^[1] and Sr-O^[2] distances show small variations with the glass composition, despite nearly constant a coordination number (~7-8) for Sr for both glass series. Such values of the coordination number are close to those observed in crystalline phases formed in transparent polycrystalline ceramics obtained from crystallization of the studied glasses used as precursors.²⁵ MD shows here that the glassy state shares many of the structural features with the crystalline phases which exhibits structural disorder in term of Al/Si mixing.

All differences observed between the two potential sets studied, using a Buckingham and Morse for the short-range interactions, can be essentially related to the differences in the predicted O^[n] populations (n=1,2,3). Indeed analysis of the strontium coordination number in terms of O^[n] with a preference factor P accounting for the O^[n] population shows that both are equivalent for O^[1] and O^[2], and similar for O^[3]. In the same vein, identical Al/Si mixing is found with the same kind of analysis. This suggests that the form of the short-range interactions control the O^[n] populations whereas Coulombic interactions (which are the same for the two models) directly impact other aspects of the structure such as the Al/Si mixing and Sr-O^[n] contact. As observed for other aluminosilicate glasses, Si-O^[2]-Al pairs are favored whereas Al-O^[1] bond is largely disfavored with respects to Si-O^[1] ones.

Concerning tricoordinated oxygens O^[3], they are mainly present in small rings, four- (edge-sharing) and six-membered, whereas AlO₅ dominantly contribute to form edge-sharing configurations. The fact that the two potential sets share these features is indicative that Al-O^[3] pairing could be governed by Coulombic interactions, thus ensuring a localized charge

equilibration at highly constraint points in the glass network. Preliminary analysis of the distribution of these points in large boxes suggest that they are non-homogenously distributed. Detailed analysis of the structure during the quench should shed light on their formation mechanisms.

To confirm our observations, ab-initio molecular dynamics simulations are pursued as well as DFT computation of NMR parameters to further assess our MD models.

Supporting Information

Derivation of the Sr-O interaction Potentials in the Buckingham form, Figure S1; Fit of the ^{27}Al MAS and MQMAS NMR spectra, Figures S2-S7; ^{27}Al NMR parameters, Tables S1-S2; ^{29}Si NMR parameters, Table S3; Calculations of the total structure factor from MD simulations; Experimental Neutron Structure factors, Figures S8-S9; Variations of bond lengths with glass composition, Figures S10-S11; Variations of Sr-O distances with glass compositions, Figure S12; O-Sr-O angle distributions, Figure S13; O-Si-O bond angle distributions, Figure S14; Variation of TBO / NBO with AlO_5 , Figure S15; Al/Si Mixing, Figures S16-S18.

Acknowledgements

This research was conducted under funding from the ANR DyStrAS (Dynamics and Structure of Aluminosilicate glasses) project (ANR-13-BS08-0012).

References

- (1) Allwardt, J. R.; Lee, S. K.; Stebbins, J. F. Bonding Preferences of Non-Bridging O Atoms: Evidence from O-17 MAS and ^{29}Si MQMAS NMR on Calcium Aluminate and Low-Silica Ca-Aluminosilicate Glasses. *Am. Mineral.* **2003**, *88*, 949–954.
- (2) Bauchy, M. Structural, Vibrational, and Elastic Properties of a Calcium Aluminosilicate Glass from Molecular Dynamics Simulations: The Role of the Potential. *J. Chem. Phys.* **2014**, *141*, 024507.

- (3) Bouhadja, M.; Jakse, N.; Pasturel, A. Structural and Dynamic Properties of Calcium Aluminosilicate Melts: A Molecular Dynamics Study. *J. Chem. Phys.* **2013**, *138*, 224510.
- (4) Cormier, L.; Ghaleb, D.; Neuville, D. R.; Delaye, J.-M.; Calas, G. Chemical Dependence of Network Topology of Calcium Aluminosilicate Glasses: A Computer Simulation Study. *J. Non-Cryst. Solids* **2003**, *332*, 255–270.
- (5) Gambuzzi, E.; Pedone, A.; Menziani, M. C.; Angeli, F.; Florian, P.; Charpentier, T. Calcium Environment in Silicate and Aluminosilicate Glasses Probed by ^{43}Ca MQMAS NMR Experiments and MD-GIPAW Calculations. *Solid State Nucl. Magn. Reson.* **2015**, *68–69*, 31–36.
- (6) Gambuzzi, E.; Pedone, A.; Menziani, M. C.; Angeli, F.; Caurant, D.; Charpentier, T. Probing Silicon and Aluminium Chemical Environments in Silicate and Aluminosilicate Glasses by Solid State NMR Spectroscopy and Accurate First-Principles Calculations. *Geochim. Cosmochim. Acta* **2014**, *125*, 170–185.
- (7) Ganster, P.; Benoit, M.; Kob, W.; Delaye, J.-M. Structural Properties of a Calcium Aluminosilicate Glass from Molecular-Dynamics Simulations: A Finite Size Effects Study. *J. Chem. Phys.* **2004**, *120*, 10172–10181.
- (8) Jakse, N.; Bouhadja, M.; Kozaily, J.; Drewitt, J. W. E.; Hennet, L.; Neuville, D. R.; Fischer, H. E.; Cristiglio, V.; Pasturel, A. Interplay between Non-Bridging Oxygen, Triclusters, and Fivefold Al Coordination in Low Silica Content Calcium Aluminosilicate Melts. *Appl. Phys. Lett.* **2012**, *101*, 201903.
- (9) Moesgaard, M.; Keding, R.; Skibsted, J.; Yue, Y. Evidence of Intermediate-Range Order Heterogeneity in Calcium Aluminosilicate Glasses. *Chem. Mater.* **2010**, *22*, 4471–4483.
- (10) Neuville, D. R.; Cormier, L.; Massiot, D. Al Coordination and Speciation in Calcium Aluminosilicate Glasses: Effects of Composition Determined by ^{27}Al MQ-MAS NMR and Raman Spectroscopy. *Chem. Geol.* **2006**, *229*, 173–185.
- (11) Lee, S. K.; Stebbins, J. F. The Degree of Aluminum Avoidance in Aluminosilicate Glasses. *Am. Mineral.* **1999**, *84*, 937–945.
- (12) Stebbins, J. F.; Dubinsky, E. V.; Kanehashi, K.; Kelsey, K. E. Temperature Effects on Non-Bridging Oxygen and Aluminum Coordination Number in Calcium Aluminosilicate Glasses and Melts. *Geochim. Cosmochim. Acta* **2008**, *72*, 910–925.
- (13) Stebbins, J. F.; Lee, S. K.; Oglesby, J. V. Al-O-Al Oxygen Sites in Crystalline Aluminates and Aluminosilicate Glasses; High-Resolution Oxygen-17 NMR Results. *Am. Mineral.* **1999**, *84*, 983–986.
- (14) Stebbins, J. F.; Xu, Z. NMR Evidence for Excess Non-Bridging Oxygen in an Aluminosilicate Glass. *Nature* **1997**, *390*, 60–62.
- (15) Neuville, D. R.; Cormier, L.; Massiot, D. Al Environment in Tectosilicate and Peraluminous Glasses: A ^{27}Al MQ-MAS NMR, Raman, and XANES Investigation. *Geochim. Cosmochim. Acta* **2004**, *68*, 5071–5079.
- (16) Skinner, L. B.; Barnes, A. C.; Salmon, P. S.; Fischer, H. E.; Drewitt, J. W. E.; Honkimäki, V. Structure and Triclustering in Ba-Al-O Glass. *Phys. Rev. B* **2012**, *85*, 064201.
- (17) Stebbins, J. F.; Oglesby, J. V.; Kroeker, S. Oxygen Triclusters in Crystalline CaAl_4O_7 (Grossite) and in Calcium Aluminosilicate Glasses: O-17 NMR. *Am. Mineral.* **2001**, *86*, 1307–1311.
- (18) Ganster, P.; Benoit, M.; Delaye, J.-M.; Kob, W. Structural and Vibrational Properties of a Calcium Aluminosilicate Glass: Classical Force-Fields vs. First-Principles. *Mol. Simul.* **2007**, *33*, 1093.

- (19) Liu, M.; Jacob, A.; Schmetterer, C.; Masset, P. J.; Hennet, L.; Fischer, H. E.; Jad Kozaily; Jahn, S.; Gray-Weale, A. From Atomic Structure to Excess Entropy: A Neutron Diffraction and Density Functional Theory Study of CaO–Al₂O₃–SiO₂ Melts. *J. Phys. Condens. Matter* **2016**, *28*, 135102.
- (20) Neuville, D. R.; Cormier, L.; Flank, A.-M.; Briois, V.; Massiot, D. Al Speciation and Ca Environment in Calcium Aluminosilicate Glasses and Crystals by Al and Ca K-Edge X-Ray Absorption Spectroscopy. *Chem. Geol.* **2004**, *213*, 153–163.
- (21) Gervais, C.; Profeta, M.; Babonneau, F.; Pickard, C. J.; Mauri, F. Ab Initio Calculations of NMR Parameters of Highly Coordinated Oxygen Sites in Aluminosilicates. *J. Phys. Chem. B* **2004**, *108*, 13249–13253.
- (22) Pedone, A.; Gambuzzi, E.; Menziani, M. C. Unambiguous Description of the Oxygen Environment in Multicomponent Aluminosilicate Glasses from ¹⁷O Solid State NMR Computational Spectroscopy. *J. Phys. Chem. C* **2012**, *116*, 14599–14609.
- (23) Pedone, A.; Gambuzzi, E.; Malavasi, G.; Menziani, M. C. First-Principles Simulations of the ²⁷Al and ¹⁷O Solid-State NMR Spectra of the CaAl₂Si₃O₁₀ Glass. *Theor. Chem. Acc.* **2012**, *131*, 1–11.
- (24) Alahraché, S.; Saghir, K. A.; Chenu, S.; Véron, E.; Meneses, D. D. S.; Becerro, A. I.; Ocaña, M.; Moretti, F.; Patton, G.; Dujardin, C.; et al. Perfectly Transparent Sr₃Al₂O₆ Polycrystalline Ceramic Elaborated from Glass Crystallization, *Chem. Mater.* **2013**, *25*, 4017–4024.
- (25) Saghir, K. A.; Chenu, S.; Veron, E.; Fayon, F.; Suchomel, M.; Genevois, C.; Porcher, F.; Matzen, G.; Massiot, D.; Allix, M. Transparency through Structural Disorder: A New Concept for Innovative Transparent Ceramics, *Chem. Mater.* **2015**, *27*, 508–514
- (26) Sharma, K.; Kothiyal, G. P.; Montagne, L.; Méar, F. O.; Revel, B. A New Formulation of Barium–strontium Silicate Glasses and Glass-Ceramics for High-Temperature Sealant. *Int. J. Hydrog. Energy* **2012**, *37*, 11360–11369.
- (27) Hyatt, M. J.; Bansal, N. P. Crystal Growth Kinetics in BaOAl₂O₃2SiO₂ and SrOAl₂O₃2SiO₂ Glasses. *J. Mater. Sci.* **1996**, *31*, 172–184.
- (28) Beall, G. H. Refractory Glass–ceramics Based on Alkaline Earth Aluminosilicates. *J. Eur. Ceram. Soc.* **2009**, *29*, 1211–1219.
- (29) Cormier, L.; Calas, G.; Creux, S.; Gaskell, P. H.; Bouchet-Fabre, B.; Hannon, A. C. Environment around Strontium in Silicate and Aluminosilicate Glasses. *Phys. Rev. B* **1999**, *59*, 13517–13520.
- (30) McKeown, D. A.; Kot, W. K.; Pegg, I. L. X-Ray Absorption Studies of the Local Strontium Environments in Borosilicate Waste Glasses. *J. Non-Cryst. Solids* **2003**, *317*, 290–300.
- (31) Novikov, A. N.; Neuville, D. R.; Hennet, L.; Gueguen, Y.; Thiaudière, D.; Charpentier, T.; Florian, P. Al and Sr Environment in Tectosilicate Glasses and Melts: Viscosity, Raman and NMR Investigation. *Chem. Geol.* **2017**, *461*, 115–127.
- (32) Park, S. Y.; Lee, S. K. High-Resolution Solid-State NMR Study of the Effect of Composition on Network Connectivity and Structural Disorder in Multi-Component Glasses in the Diopside and Jadeite Join: Implications for Structure of Andesitic Melts. *Geochim. Cosmochim. Acta* **2014**, *147*, 26–42.
- (33) Stebbins, J. F.; Wu, J.; Thompson, L. M. Interactions between Network Cation Coordination and Non-Bridging Oxygen Abundance in Oxide Glasses and Melts: Insights from NMR Spectroscopy. *Chem. Geol.* **2013**, *346*, 34–46.

- (34) Thompson, L. M.; Stebbins, J. F. Non-Stoichiometric Non-Bridging Oxygens and Five-Coordinated Aluminum in Alkaline Earth Aluminosilicate Glasses: Effect of Modifier Cation Size. *J. Non-Cryst. Solids* **2012**, *358*, 1783–1789.
- (35) Jaworski, A.; Stevansson, B.; Edén, M. The Bearings from Rare-Earth (RE = La, Lu, Sc, Y) Cations on the Oxygen Environments in Aluminosilicate Glasses: A Study by Solid-State ¹⁷O NMR, Molecular Dynamics Simulations, and DFT Calculations. *J. Phys. Chem. C* **2016**, *120*, 13181–13198.
- (36) Jaworski, A.; Stevansson, B.; Edén, M. Direct ¹⁷O NMR Experimental Evidence for Al–NBO Bonds in Si-Rich and Highly Polymerized Aluminosilicate Glasses. *Phys. Chem. Chem. Phys.* **2015**, *17*, 18269–18272.
- (37) Hennet, L.; Pozdnyakova, I.; Bytchkov, A.; Cristiglio, V.; Palleau, P.; Fischer, H. E.; Cuello, G. J.; Johnson, M.; Melin, P.; Zanghi, D.; et al. Levitation Apparatus for Neutron Diffraction Investigations on High Temperature Liquids. *Rev. Sci. Instrum.* **2006**, *77*, 053903.
- (38) Massiot, D.; Touzo, B.; Trumeau, D.; Coutures, J. P.; Virlet, J.; Florian, P.; Grandinetti, P. J. Two-Dimensional Magic-Angle Spinning Isotropic Reconstruction Sequences for Quadrupolar Nuclei. *Solid State Nucl. Magn. Reson.* **1996**, *6*, 73–83.
- (39) Carr, H. Y.; Purcell, E. M. Effects of Diffusion on Free Precession in Nuclear Magnetic Resonance Experiments. *Phys. Rev.* **1954**, *94*, 630–638.
- (40) Larsen, F. H.; Farnan, I. ²⁹Si and ¹⁷O (Q)CPMG-MAS Solid-State NMR Experiments as an Optimum Approach for Half-Integer Nuclei Having Long T₁ Relaxation Times. *Chem. Phys. Lett.* **2002**, *357*, 403–408.
- (41) Meiboom, S.; Gill, D. Modified Spin-Echo Method for Measuring Nuclear Relaxation Times. *Rev. Sci. Instrum.* **1958**, *29*, 688–691.
- (42) Fischer, H. E.; Cuello, G. J.; Palleau, P.; Feltn, D.; Barnes, A. C.; Badyal, Y. S.; Simonson, J. M. D4c: A Very High Precision Diffractometer for Disordered Materials. *Appl. Phys. A* **2002**, *74*, s160–s162.
- (43) Cuello, G. J. Structure Factor Determination of Amorphous Materials by Neutron Diffraction. *J. Phys. Condens. Matter* **2008**, *20*, 244109.
- (44) A, H. M.; L, M. R.; P, Z. *CORRECT: A Correction Program for Neutron Diffraction Data*; NFL, Uppsala University, 1996.
- (45) Smith, W.; Forester, T. R. DL_POLY_2.0: A General-Purpose Parallel Molecular Dynamics Simulation Package. *J. Mol. Graph.* **1996**, *14*, 136–141.
- (46) Todorov, I. T.; Smith, W.; Trachenko, K.; Dove, M. T. DL_POLY_3: New Dimensions in Molecular Dynamics Simulations via Massive Parallelism. *J. Mater. Chem.* **2006**, *16*, 1911–1918.
- (47) Pedone, A.; Malavasi, G.; Menziani, M. C.; Cormack, A. N.; Segre, U. A New Self-Consistent Empirical Interatomic Potential Model for Oxides, Silicates, and Silica-Based Glasses. *J. Phys. Chem. B* **2006**, *110*, 11780–11795.
- (48) Du, J. Molecular Dynamics Simulations of the Structure and Properties of Low Silica Yttrium Aluminosilicate Glasses. *J. Am. Ceram. Soc.* **2009**, *92*, 87–95.
- (49) Du, J.; Cormack, A. N. The Structure of Erbium Doped Sodium Silicate Glasses. *J. Non-Cryst. Solids* **2005**, *351*, 2263–2276.
- (50) Du, J.; René Corrales, L. Understanding Lanthanum Aluminate Glass Structure by Correlating Molecular Dynamics Simulation Results with Neutron and X-Ray Scattering Data. *J. Non-Cryst. Solids* **2007**, *353*, 210–214.

- (51) Okhotnikov, K.; Stevansson, B.; Edén, M. New Interatomic Potential Parameters for Molecular Dynamics Simulations of Rare-Earth (RE = La, Y, Lu, Sc) Aluminosilicate Glass Structures: Exploration of RE³⁺ Field-Strength Effects. *Phys. Chem. Chem. Phys.* **2013**, *15*, 15041–15055.
- (52) Florian, P.; Veron, E.; Green, T. F. G.; Yates, J. R.; Massiot, D. Elucidation of the Al/Si Ordering in Gehlenite Ca₂Al₂SiO₇ by Combined ²⁹Si and ²⁷Al NMR Spectroscopy/Quantum Chemical Calculations. *Chem. Mater.* **2012**, *24*, 4068–4079.
- (53) Duxson, P.; Provis, J. L.; Lukey, G. C.; Separovic, F.; van Deventer, J. S. J. ²⁹Si NMR Study of Structural Ordering in Aluminosilicate Geopolymer Gels. *Langmuir* **2005**, *21*, 3028–3036.
- (54) Hiet, J.; Deschamps, M.; Pellerin, N.; Fayon, F.; Massiot, D. Probing Chemical Disorder in Glasses Using Silicon-29 NMR Spectral Editing. *Phys. Chem. Chem. Phys.* **2009**, *11*, 6935–6940.
- (55) Provis, J. L.; Duxson, P.; Lukey, G. C.; van Deventer, J. S. J. Statistical Thermodynamic Model for Si/Al Ordering in Amorphous Aluminosilicates. *Chem. Mater.* **2005**, *17*, 2976–2986.
- (56) Angeli, F.; Villain, O.; Schuller, S.; Ispas, S.; Charpentier, T. Insight into Sodium Silicate Glass Structural Organization by Multinuclear NMR Combined with First-Principles Calculations. *Geochim. Cosmochim. Acta* **2011**, *75*, 2453–2469.
- (57) Bernasconi, A.; Dapiaggi, M.; Pavese, A.; Bowron, D. T.; Imberti, S. Local Structure of Si-Al-Ca-Na-O Glasses from Coupled Neutron and X-Ray Total Scattering Data. *J. Phys. Chem. B* **2012**, *116*, 13114–13123.
- (58) Shimoda, K.; Tobu, Y.; Hatakeyama, M.; Nemoto, T.; Saito, K. Structural Investigation of Mg Local Environments in Silicate Glasses by Ultra-High Field ²⁵Mg 3QMAS NMR Spectroscopy. *Am. Mineral.* **2007**, *92*, 695–698.
- (59) Xiang, Y.; Du, J.; Smedskjaer, M. M.; Mauro, J. C. Structure and Properties of Sodium Aluminosilicate Glasses from Molecular Dynamics Simulations. *J. Chem. Phys.* **2013**, *139*, 044507.
- (60) Zheng, Q.; Smedskjaer, M. M.; Youngman, R. E.; Potuzak, M.; Mauro, J. C.; Yue, Y. Influence of Aluminum Speciation on the Stability of Aluminosilicate Glasses against Crystallization. *Appl. Phys. Lett.* **2012**, *101*, 041906-041906–4.
- (61) Charpentier, T.; Ispas, S.; Profeta, M.; Mauri, F.; Pickard, C. J. First-Principles Calculation of ¹⁷O, ²⁹Si, and ²³Na NMR Spectra of Sodium Silicate Crystals and Glasses. *J. Phys. Chem. B* **2004**, *108*, 4147–4161.
- (62) Tilocca, A.; de Leeuw, N. H.; Cormack, A. N. Shell-Model Molecular Dynamics Calculations of Modified Silicate Glasses. *Phys. Rev. B* **2006**, *73*, 104209.
- (63) Benoit, M.; Ispas, S.; Tuckerman, M. E. Structural Properties of Molten Silicates from Ab Initio Molecular-Dynamics Simulations: Comparison between CaO-Al₂O₃-SiO₂ and SiO₂. *Phys. Rev. B* **2001**, *64*, 224205.
- (64) Lee, S. K.; Stebbins, J. F. Disorder and the Extent of Polymerization in Calcium Silicate and Aluminosilicate Glasses: O-17 NMR Results and Quantum Chemical Molecular Orbital Calculations. *Geochim. Cosmochim. Acta* **2006**, *70*, 4275–4286.
- (65) Bonhomme, C.; Gervais, C.; Folliet, N.; Pourpoint, F.; Coelho Diogo, C.; Lao, J.; Jallot, E.; Lacroix, J.; Nedelec, J.-M.; Iuga, D.; et al. ⁸⁷Sr Solid-State NMR as a Structurally Sensitive Tool for the Investigation of Materials: Antiosteoporotic Pharmaceuticals and Bioactive Glasses. *J. Am. Chem. Soc.* **2012**, *134*, 12611–12628.

- (66) Xiang, Y.; Du, J. Effect of Strontium Substitution on the Structure of 45S5 Bioglasses. *Chem. Mater.* **2011**, *23*, 2703–2717.
- (67) Jaworski, A.; Stevansson, B.; Pahari, B.; Okhotnikov, K.; Edén, M. Local Structures and Al/Si Ordering in Lanthanum Aluminosilicate Glasses Explored by Advanced ^{27}Al NMR Experiments and Molecular Dynamics Simulations. *Phys. Chem. Chem. Phys.* **2012**, *14*, 15866–15878.
- (68) Stevansson, B.; Jaworski, A.; Edén, M. The Structural Roles of Sc and Y in Aluminosilicate Glasses Probed by Molecular Dynamics Simulations. *J. Non-Cryst. Solids* **2017**, *460*, 36–46.
- (69) Lee, S. K.; Stebbins, J. F. Al–O–Al and Si–O–Si Sites in Framework Aluminosilicate Glasses with Si/Al=1: Quantification of Framework Disorder. *J. Non-Cryst. Solids* **2000**, *270*, 260–264.
- (70) Lee, S. K.; Stebbins, J. F. Effects of the Degree of Polymerization on the Structure of Sodium Silicate and Aluminosilicate Glasses and Melts: An ^{17}O NMR Study. *Geochim. Cosmochim. Acta* **2009**, *73*, 1109–1119.
- (71) Christie, J. K.; Tilocca, A. Aluminosilicate Glasses As Yttrium Vectors for in Situ Radiotherapy: Understanding Composition-Durability Effects through Molecular Dynamics Simulations. *Chem. Mater.* **2010**, *22*, 3725–3734.